Thermal Activation of Superconducting Josephson Junctions

by

Aditya P. Devalapalli

Submitted to the Department of Physics
in partial fulfillment of the requirements for the degree of

Bachelor of Science in Physics

at the

MASSACHUSETTS INSTITUTE OF TECHNOLOGY

May 2007
[June 2007]

© Aditya P. Devalapalli, MMVII. All rights reserved.

The author hereby grants to MIT permission to reproduce and distribute publicly paper and electronic copies of this thesis document in whole or in part.

Author .....
Department of Physics
18 May 2007

Certified by .....
Leonid Levitov
Professor, Department of Physics
Thesis Supervisor

Certified by .....
William D. Oliver
Research Associate, MIT Lincoln Laboratory
Thesis Supervisor

Accepted by .....
David E. Pritchard
Senior Thesis Coordinator, Department of Physics

MASSACHUSETTS INSTITUTE OF TECHNOLOGY
AUG 0 6 2007
LIBRARIES

ARCHIVES

Thermal Activation of Superconducting Josephson Junctions

by

Aditya P. Devalapalli

Submitted to the Department of Physics
on 18 May 2007, in partial fulfillment of the
requirements for the degree of
Bachelor of Science in Physics

Abstract

Superconducting quantum circuits (SQCs) are being explored as model systems for scalable quantum computing architectures. Josephson junctions are extensively used in superconducting quantum interference devices (SQUIDs) and in persistent-current qubit systems. Noise excitations, however, have a critical influence on their dynamics. Thus, the primary focus of this research was to investigate the effects of thermal activation on the superconducting properties of Josephson junctions. Specifically, thermal noise tends to result in a range of switching currents, values less than the critical current at which a junction switches from the superconducting to the normal state. First, a general review of superconductivity concepts is given, including a treatment of the Josephson phenomena. Next, I describe some of my work on characterizing the current-voltage traces of Josephson junctions tested at 4 K with a Multi-Chip Probe (MCP). Then, I describe thermal activation theory and examine the equations useful for modeling switching current distributions. The Josephson junctions of a SQUID with a ramped bias current were tested for numerous temperatures $T \leq 4.5$ K (and with various magnetic flux frustrations). Fit parameters of critical current, capacitance, resistance, and temperature were determined from modeling the escape rates and switching current probability distributions. The thermal activation model succeeded in fitting the results to good agreement, where parameters $C = 2.000 \pm 0.002$ pF and $T = 1.86 \pm 0.06$ K were obtained for 1.8 K data. For significantly lower temperatures, the model tends to predict higher than expected temperatures; further analysis would need to include the quantum mechanical tunneling model better in the fitting scheme.

Thesis Supervisor: Leonid Levitov
Title: Professor, Department of Physics

Thesis Supervisor: William D. Oliver
Title: Research Associate, MIT Lincoln Laboratory

Acknowledgments

First and foremost, I would like to thank my mentor, William Oliver, for giving me the opportunity to be an integral member of the research process at MIT Lincoln Laboratory. His patience and guidance have helped me to learn and grow as a student, as well as to always keep asking questions as an investigator. Keith Brown has been a role model for me in the laboratory, and I am very thankful for his wisdom, advice, and friendship. I am also grateful to Terry Weir for his technical support in many of the projects I worked on. Jeremy Sage and David Berns have been most gracious in extending their help to me, and I would particularly like to thank David for his assistance on the data analysis. I am indebted to Prof. Terry Orlando for his advice and support, as well as to Prof. Leonid Levitov for helping to review this thesis. Finally, I would like to thank Gerald Dionne for his cheerful company.

Contents

List of Figures

List of Tables

Chapter 1

Introduction

1.1 Motivation

H. Kammerlingh Onnes' discovery in 1911 of vanishing electrical resistance in a cooled mercury sample yielded the first example of superconductivity [1]. Since then, the phenomenon of superconductivity has had many far-reaching implications for condensed matter physics. While the resistivity in normal metal conductors gradually diminishes as the temperature is lowered, the resistance never completely vanishes. Superconductors, however, are characterized by a drastic drop to exactly zero electrical resistance below some critical temperature T_c ($T_c < 20$ K for most ordinary superconductors). Thus, currents in superconductors could theoretically persist forever without any appreciable decrease due to the absence of resistance. In 1933, Meissner and Ochsenfeld demonstrated that superconductors also actively expel all external magnetic fields from their interior [2], an effect which was later explained by the London equations. Then, in 1957, Bardeen, Cooper, and Schrieffer formulated the microscopic theory of superconductivity [3], whose effects could be observed on the macroscopic scale.

We now know that superconductivity is not merely the perfect limit of classical conductivity but that it is a special thermodynamic phase correctly described by quantum mechanics. Today, superconductors are employed in the world's most powerful electromagnets, such as magnetic resonance imaging (MRI) machines and

particle accelerators. They are also used to make sensitive measurements of the magnetic flux quantum, $\Phi_0 = hc/2e$, in unique magnetometers called superconducting quantum interference devices (SQUIDs).

Superconducting quantum circuits (SQCs) are now sought after as model components for quantum computing [4]. These macroscopic systems are based on special thin insulating barriers (~10 Å) separating two superconducting materials called Josephson junctions. They can be driven by external fields and demonstrate quantum two-state dynamics, making them ideal candidates for quantum bits, or qubits [5]. Just as conventional computers process bit logic (0 or 1) with transistors, quantum computers can store information in quantum variables using qubits. SQCs are promising qubit systems because of their ease of design, fabrication, and scalability. However, there are still major challenges towards reducing decoherence times and controlling the dynamics of SQCs before they can be realized in a large-scale quantum computer. My goal is to evaluate some of the dynamics of these devices and be able to extract important parameters of their superconducting properties.

1.2 Overview of Applications

Superconductivity was initially only exhibited in certain metals when cooled to liquid helium temperatures (4.2 K). Helium cooling is quite complex and expensive, however; advanced helium dilution refrigerators today are capable of cooling down to ~10 mK but are costly to build and maintain. Fortunately, discoveries during the 1980s revealed superconductivity at much warmer critical temperatures in ceramic materials such as $LaBa_2CuO_{4-x}$ (30 K) [6], $YBa_2Cu_3O_x$ (93 K) [7], and $Hg_2Ba_2Ca_2Cu_3O_x$ (130 K) [8]. Since liquid nitrogen cools at 77 K, these new high-T_c materials could achieve superconductivity with cheaper, alternative methods to liquid helium cooling. High-temperature superconductors (HTS) now have significant roles in electric power applications as superconducting magnetic energy storage devices, power cables, and transformers. Further advances in this technology have implemented cheaper and more abundant metals (e.g. Cu, Fe, Mg, B) in HTS alloys, which have promoted

their use in research and in industry. [9]

Josephson junctions have also stirred significant interest with their important applications to SQCs. Josephson junctions permit superconducting current to pass through in the form of quasi-particle (electron) tunneling when cooled to sufficiently low temperatures $T < T_c$. The nonlinear dynamics and other unique properties of Josephson junctions make them suitable for implementation in SQCs. Two Josephson junctions in parallel can be fashioned in a superconducting ring that can detect infinitesimal changes in magnetic flux at the scale of a single flux quantum, Φ_0. These aforementioned devices are known as SQUIDs, and because of their incredible precision, they are commonly used as magnetometers for sensing minute magnetic fields [10], such as those generated in living organisms. Superconducting Josephson junctions have also found numerous other uses as infrared detectors, microwave generators, voltmeters, computer logic and memory devices, oscillators, and spectrometers [11].

1.3 Current Research Efforts

Great strides are continuing to be made towards realizing fully functional qubits for use in quantum computing. The strong collaboration between MIT Lincoln Laboratory and Prof. Terry Orlando's group at MIT's Research Laboratory of Electronics (RLE) attests to the commitment in improving the design, fabrication, and testing of SQCs. Their ongoing research efforts have already yielded exciting knowledge about Josephson junctions and their performance in SQUIDs and persistent-current (PC) qubits. They have thoroughly investigated energy relaxation times [12][13], decoherence [14], inductance effects [15], microwave-induced cooling [16], resonant readouts [17], and other dynamics of niobium PC qubits using Josephson junctions [18][19]. They continue to study and enhance these qubits as model systems for scalable quantum computing architectures [20][21].

I have been working at MIT Lincoln Laboratory under the mentorship of Dr. William D. Oliver, who collaborates extensively with the Orlando group at RLE. I developed software that evaluates the current-voltage characteristics of Josephson

junctions tested with various probes at cryogenic temperatures. I also accumulated the results in a novel database management system and built wafer maps from aggregate data that has helped to improve the custom design and fabrication process of Josephson junction chips produced at MIT Lincoln Laboratory. A major concern when testing SQCs is determining the effects of noise on the device performance. The presence of thermal noise can produce undesirable consequences for Josephson junctions, which can be excited from their ground superconducting states to their normal conducting states. These switching events can occur randomly within a range of bias currents depending on the temperature and the magnetic flux applied to the SQUID. The primary focus of my investigation has been analyzing the switching current distributions of SQUID junctions under a ramped bias current tested at various temperatures $T \leq 4.5$ K. I attempt to use thermal activation theory to extract relevant parameters from the distributions, such as the critical current, capacitance, resistance, and temperature. Finally, I describe future work where quantum mechanical tunneling can potentially explain aspects of the switching current dynamics at base temperatures ($T < 50$ K) when the thermal activation model breaks down.

Chapter 2

Theory of Superconductivity

2.1 The Meissner Effect

To understand superconducting quantum circuits, it is fitting that we begin with a review of superconductivity. Much of the treatment here is taken directly from Tinkham [22], Solymar [23], and Kittel [24]. One of the defining characteristics of superconductors is that when cooled to below some critical temperature, usually a few degrees Kelvin, they enter into the superconducting phase characterized by absolutely zero electrical resistance. Superconductors also possess the unique ability to eliminate any externally magnetic fields from their interior (see Fig. 2-1(a)). If a normal conductor were cooled to a state of zero electrical resistance, any external magnetic field would be sustained through the conductor's interior. If a magnetic field is applied to a superconductor above its critical temperature, the field penetrates through the material, but once it is cooled and enters its superconducting phase, all internal flux is completely expelled by the emergence of circulating surface currents that perfectly cancel the external field. This phenomenon, distinct from mere perfect diamagnetism with zero resistance, is peculiar to superconductors alone and is known as the Meissner effect. The principle of the Meissner effect was later correctly explained by the London equations, which will be described in the next section.

Just as superconductivity can be destroyed beyond a critical temperature, the reverse Meissner effect can occur beyond a critical magnetic field. For a given tem-

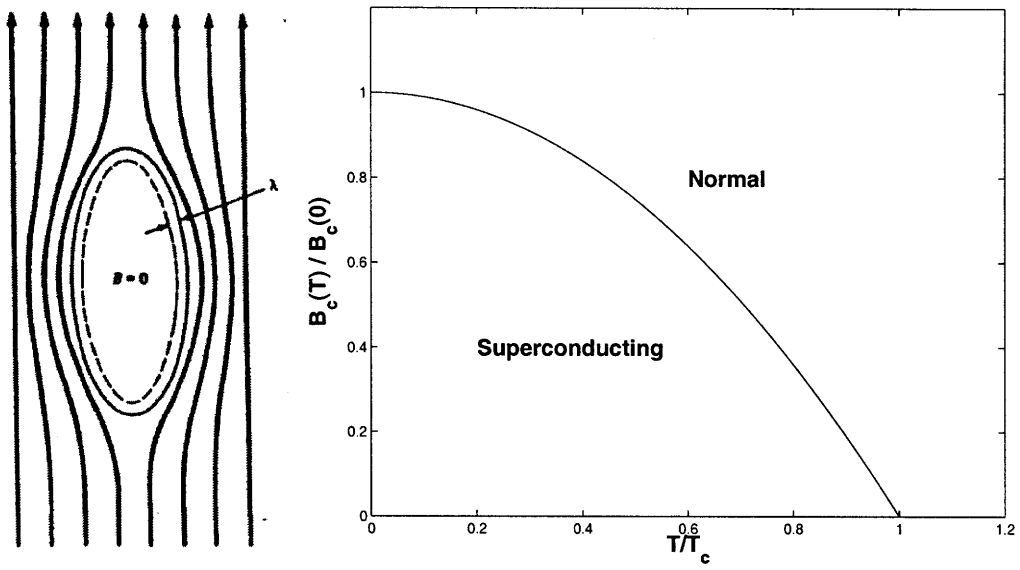

(a) The Meissner effect

(b) The critical magnetic field

Figure 2-1: Effects of magnetic field on a superconductor. (a) Upon transitioning to below T_c, any external magnetic field is expelled from the interior with London penetration depth λ_L at the superconductor surface. (Figure reproduced from Tinkham.) (b) Parabolic relationship between critical magnetic field B_c and temperature that divides the normal and superconducting states.

perature $T < T_c$, a certain magnetic field strength provides exactly enough magnetic energy to make up the free energy difference between the normal and superconducting states. This principle is well approximated by the parabolic relationship

$$B_c(T) \approx B_c(0)(1 - (T/T_c)^2) \tag{2.1}$$

which is illustrated in Fig. 2-1(b)

Type I superconductors are bulk materials that completely repel any internal magnetic fields from their interior. However, materials that possess some impurities permit magnetic fields to penetrate through holes, or filaments, along the length of the superconducting interior. The filaments are regions in the normal conducting state and are surrounded by vortices of superconducting current. These materials

are known as Type II superconductors. They act perfectly diamagnetic up to a certain critical field B_{c1}, just like Type I superconductors, but then permit partial flux penetration gradually up to a higher critical field B_{c2}, beyond which superconductivity is completely destroyed. Type II superconductors, thus, are distinguished by their mixed-state Meissner effect between B_{c1} and B_{c2} where superconductivity can be sustained at higher fields while gradually broken down.

2.2 The London Equations

F. and H. London were able to explain the findings of Meissner and Ochsenfeld [25]. They first assumed that conduction electrons in the superconductor carry the persistent supercurrent without any friction, or resistance. The electron motion for perfect conductivity is described by

$$m\frac{d\mathbf{v}}{dt} = -e\mathbf{E}. \tag{2.2}$$

The supercurrent density, given by $\mathbf{J} = -n_s e\mathbf{v}$ where n_s is the superconducting electron density, can now be combined with the equation of motion to yield the first London equation:

$$\Lambda\frac{\partial \mathbf{J}}{\partial t} = \mathbf{E}; \qquad \Lambda = \frac{m}{n_s e^2}. \tag{2.3}$$

The London brothers realized that the above equation merely defines what they called the "acceleration theory", which just describes electron acceleration without friction. They took their first equation as a starting point for discovering where superconductivity fundamentally deviates from normal conductivity. Coupling Eq. 2.3 with the Maxwell equations $\nabla \times \mathbf{E} = -(1/c)\partial\mathbf{B}/\partial t$ and $\nabla \times \mathbf{B} = (4\pi/c)\mathbf{J}$, we arrive at the equation

$$\nabla \times \left(\nabla \times \Lambda\frac{\partial \mathbf{B}}{\partial t}\right) = -\frac{4\pi}{c^2}\frac{\partial \mathbf{B}}{\partial t}. \tag{2.4}$$

Now using the vector identity $\nabla \times (\nabla \times \mathbf{C}) = \nabla(\nabla \cdot \mathbf{C}) - (\nabla \cdot \nabla)\mathbf{C}$ and the Maxwell equation $\nabla \cdot \mathbf{B} = 0$, we obtain

$$\Lambda\nabla^2\frac{\partial \mathbf{B}}{\partial t} = \frac{4\pi}{c^2}\frac{\partial \mathbf{B}}{\partial t}. \tag{2.5}$$

Finally, integrating with respect to time, we immediately find that one particular solution to this equation is $\partial \mathbf{B}/\partial t = 0$ or $\mathbf{B} = \mathbf{B}_0$, which maintains the initial magnetic field at time $t = 0$ for all time t. This is true for normal conductors with no electrical resistance, but we know that all applied magnetic field is quenched from the interior in superconductors due to the Meissner effect.

Since Eq. 2.3 alone is inadequate to describe the effects of a magnetic field on superconductors, the London brothers subsequently reverted to a more quantum mechanical approach. Using the vector potential $\mathbf{A}$ and the canonical momentum $\mathbf{p} = m\mathbf{v} - e\mathbf{A}/c$ for electrons, F. and H. London assumed that the superconducting ground state is characterized by zero net momentum $\langle \mathbf{p} \rangle = 0$. Therefore, the average velocity of superconducting electrons is

$$\langle \mathbf{v}_s \rangle = \frac{e}{mc}\mathbf{A}. \tag{2.6}$$

The definition of the supercurrent density now gives us a much more fundamental equation:

$$\mathbf{J} = -n_s e \langle \mathbf{v}_s \rangle = -\frac{n_s e^2}{mc}\mathbf{A} = -\frac{1}{\Lambda c}\mathbf{A}. \tag{2.7}$$

If we use the particular gauge $\nabla \cdot \mathbf{A} = 0$ (also known as the London gauge), then the time derivative of the above equation yields the first London equation (Eq. 2.3) and the curl yields the more significant second London equation:

$$\nabla \times (\Lambda \mathbf{J}) = -\frac{1}{c}\mathbf{B}. \tag{2.8}$$

Extending the second London equation with the Maxwell equations $\nabla \times \mathbf{B} = (4\pi/c)\mathbf{J}$ and $\nabla \cdot \mathbf{B} = 0$ elegantly explains the Meissner effect with

$$\nabla^2 \mathbf{B} = \frac{4\pi}{\Lambda c^2}\mathbf{B} = \frac{1}{\lambda_L^2}\mathbf{B}. \tag{2.9}$$

This equation reveals that the field $\mathbf{B}$ cannot be uniform in space unless $\mathbf{B} = 0$.

Therefore, Eq. 2.9 only has the exponential solution

$$B(z) = B(0)\exp(-z/\lambda_L), \tag{2.10}$$

indicating that the magnetic field drops quite abruptly at the surface with the characteristic depth

$$\lambda_L = \left(\frac{\Lambda c^2}{4\pi}\right)^{1/2} = \left(\frac{mc^2}{4\pi n_s e^2}\right)^{1/2}. \tag{2.11}$$

The parameter λ_L is known as the London penetration depth, qualitatively describing that the magnetic field exponentially decays at the surface and is effectively zero throughout the interior of the superconductor. Thus, the London equations were able to theoretically explain why magnetic fields are not simply "frozen in" as in normal conductors but are completely forced out in the superconducting phase.

2.3 The BCS Theory

Bardeen, Schrieffer, and Cooper (BCS) developed a powerful microscopic theory that explained the principle of superconductivity in 1957 [3]. The complete derivation of the BCS theory is quite cumbersome for any formal treatment here. I will only summarize its major findings and implications. The principal tenets of the theory are as follows:

1. The Fermi sea of electrons is unstable unless there is at least a weak attractive interaction between two electrons. Lattice deformations cause two distant electrons of opposite spin and momentum to become weakly coupled in special bound states called Cooper pairs. These electrons exchange phonons, units of vibrational energy, through the crystal lattice in the superconducting material and can thus be bound across thousands of atomic spacings.

2. The binding interaction of Cooper pairs in states ($\mathbf{k}\uparrow, -\mathbf{k}\downarrow$) leads to the existence of an energy gap between the Fermi ground state and the quasi-particle excited state of superconducting systems. Their predictions agreed well with

quantitative measurements of the energy gap. BCS formulated that this energy gap was the minimum energy $E_g = 2\Delta$ required to break apart a Cooper pair into its two constituent quasi-particles.

3. The London equations follow from the treatment of the wavefunctions for the superconducting states. Thus, the BCS assumptions were successfully able to explain the Meissner effect. They also formulated a more robust version of the London penetration depth, λ_L, that identifies the extent of magnetic field penetration. In addition, they corroborate Ginzburg-Landau (GL) theory by characterizing the separation of the electrons bound in a Cooper pair with the coherence length ξ. Treating this parameter as the inherent extension of the wavefunction that describes the center of mass motion for the Cooper pairs, they define the intrinsic coherence length

$$\xi_0 = \frac{\hbar v_F}{\pi \Delta(0)} \tag{2.12}$$

where v_F is the Fermi velocity and $\Delta(0)$ is the energy gap parameter at zero temperature. The energy gap's temperature dependence is predicted to be

$$\frac{\Delta(T)}{\Delta(0)} \approx 1.74 \left(1 - \frac{T}{T_c}\right)^{1/2}. \tag{2.13}$$

4. Since the BCS ground state involves Cooper pairs of charge $2e$, magnetic flux through a superconducting ring must be quantized in units of charge $2e$.

BCS theory is essentially based on the argument that the formation of Cooper pairs lowers the ground state energy of superconductors below that of the free electron Fermi state. Cooper pairs can produce quasi-particles (electrons) that can tunnel through from one superconductor to the next across a Josephson junction, for example, and then re-establish the bound Cooper state. This is the source of the superconducting electron tunneling, or Josephson current, that flows across a Josephson junction. Superconductive tunneling in this manner can occur at zero voltage, but if the voltage is increased to $V = E_g/2e = \Delta/e$ for normal-superconductor (NS) tun-

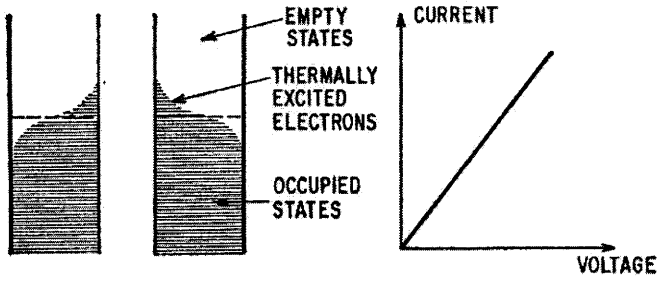

(a) NN tunneling

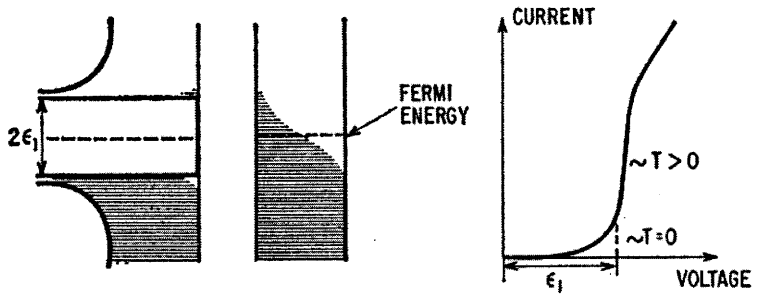

(b) NS tunneling

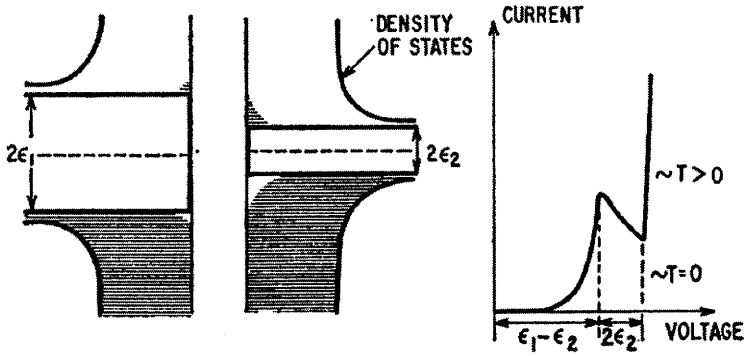

(c) SS tunneling

Figure 2-2: Electron tunneling across different barriers. (a) Normal-normal conductor (NN) tunneling exhibits a completely Ohmic current-voltage relationship. (b) Normal-superconductor (NS) tunneling occurs for $V < \epsilon_1$ at zero temperature; for higher voltages, the barrier gains a normal resistance. (c) Superconductor-superconductor (SS) tunneling across different energy gaps $2\epsilon_1$ and $2\epsilon_2$; if the superconductors are equivalent, the gap voltage is simply $V = 2\epsilon = 2\Delta/e$. (Figures reproduced from Giaever and Megerle.)

neling or to $V = \Delta/e$ for superconductor-superconductor (SS) tunneling, the ground state is broken and the barrier subsequently exhibits normal conductivity following Ohm's law. Electron tunneling between two normal conductors, a superconductor and a normal coductor, and two different superconductors is illustrated in Fig. 2-2, along with their respective current-voltage characteristics.

2.4 The Josephson Phenomena

B. D. Josephson discovered that an extremely thin (~10 Å) insulating layer between two superconducting materials permits superconducting current to pass through up to a critical current value I_c at zero voltage [26]. These devices are now known as Josephson junctions. An image of some actual junctions fabricated and tested at MIT Lincoln Laboratory is shown in Fig. 2-3(a). The BCS and GL theories helped to prove that it is simply quasi-particles from Cooper pairings that tunnel through to generate this current. Cooper pairings across the whole superconductor lower the energy of the material by a slight amount, called the "condensation energy", which is sufficient enough to lock the pairs into essentially a Bose-Einstein condensate with a common phase. This phase coherence allows us to describe the entire superconducting state with a single wavefunction and common macroscopic phase, $\psi = |\psi|e^{i\phi}$.

Now imagine two superconductors with respective phases ϕ_1 and ϕ_2 separated by a distance d of only a few atomic spacings. As $d \to 0$, the phases become coupled in a way that permits electron tunneling across the barrier. If Cooper pairs tunnel out to the same energy in the neighboring superconductor, then the DC Josephson Effect is observed. Josephson showed that in the case of weak coupling (and no magnetic field), the superconducting current density across the junction

$$J = J_c \sin\phi \tag{2.14}$$

oscillates with respect to the phase difference $\phi \equiv \phi_2 - \phi_1$ and with maximum critical current density J_c. The rate of change in ϕ is related to the potential energy difference

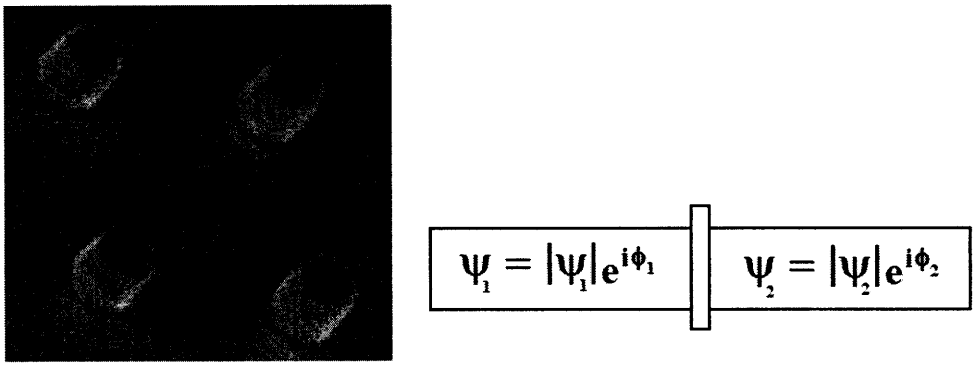

(a) Micrograph of Josephson junctions

(b) Josephson junction model

Figure 2-3: Josephson junctions. (a) Optical image of Josephson junctions fabricated and tested at MIT Lincoln Laboratory. (b) Simplified wavefunction model of Josephson junction separating two superconductors with respective macroscopic phases ϕ_1 and ϕ_2.

across the junction (in CGS units):

$$\frac{d\phi}{dt} = \frac{2e}{hc}V. \tag{2.15}$$

If the DC voltage is increased across the junction, then the current will oscillate at high frequencies but average to zero in a plot of current vs. voltage. The current remains at zero until the gap voltage $V_g = 2\Delta/e$ is reached, at which point Cooper pairs dissociate and release single electrons that exhibit normal tunneling across the junction. The junction thus gains a finite voltage and returns to its normal state, with Ohmic resistance R_n. Ambegaokar and Baratoff later discovered that for two idential superconductors, the critical current density has the temperature dependence

$$J_c = \frac{\pi\Delta(T)}{2eR_n}\tanh\left(\frac{\Delta(T)}{2k_BT}\right), \tag{2.16}$$

where $\Delta(T)$ is the temperature-dependent energy gap parameter [27].

If Cooper pairs tunnel out to a lower energy owing to differences in electrochemical

potentials, then photons are released with an energy that makes up this difference:

$$h\nu = 2eV. \tag{2.17}$$

Because the relative phase difference ϕ has a time evolution of $e^{-iEt/\hbar}$, the current I will be induced to oscillate at the corresponding frequency ν, typically at microwave levels. This is called the AC Josephson Effect, and applying a high-frequency voltage induces DC current in harmonic steps in relation to the applied frequency. First observed by Shapiro [28], these steps were found to occur at integer multiples of $h\nu/2e$.

An applied magnetic field has an important effect on the Josephson current. With a magnetic field aligned perpendicularly to the direction of current and in the plane of the Josephson junction, the zero-voltage Josephson current exhibits resonances for specific values of the external field. Thus, Eq. 2.14 can now be modified to include the gauge potential:

$$J = J_c \sin\left(\phi - \frac{2e}{\hbar c}\int \mathbf{A}\cdot d\mathbf{s}\right). \tag{2.18}$$

Integrating along a path enclosing the entire junction and using Stokes' Theorem, we find that

$$J = J_c \sin\left(\phi - 2\pi\frac{\Phi}{\Phi_0}\right), \tag{2.19}$$

where Φ is the total magnetic flux and $\Phi_0 = hc/2e$ is the magnetic flux quantum (the value Φ/Φ_0 is known as the frustration). Thus, the Josephson current should exhibit nodes at intervals of characteristic fields B_0, $2B_0$, $3B_0$, etc. In fact, the maximum supercurrent across the junction is described by

$$I_{max} = I_c\left|\frac{\sin(\pi\Phi/\Phi_0)}{\pi\Phi/\Phi_0}\right| \tag{2.20}$$

This is simply the absolute value of the first spherical Bessel function, and the current exhibits a "single slit" diffraction pattern (see Fig. 2-4(a)).

Two parallel Josephson junctions in a superconducting circuit demonstrate the best example of flux quantization. If Φ now describes the total flux through the ring

containing the two equivalent junctions, the maximum supercurrent measured in the device is given as

$$I_{max} = 2I_c \left| \cos\left(\pi \frac{\Phi}{\Phi_0}\right) \right|. \tag{2.21}$$

These instruments, as previously mentioned, are known as superconducting quantum interference devices (SQUIDs) and are practical magnetometers for sensitive measurements of the magnetic field. The DC SQUID is the primary device of interest in my study of thermal activation theory.

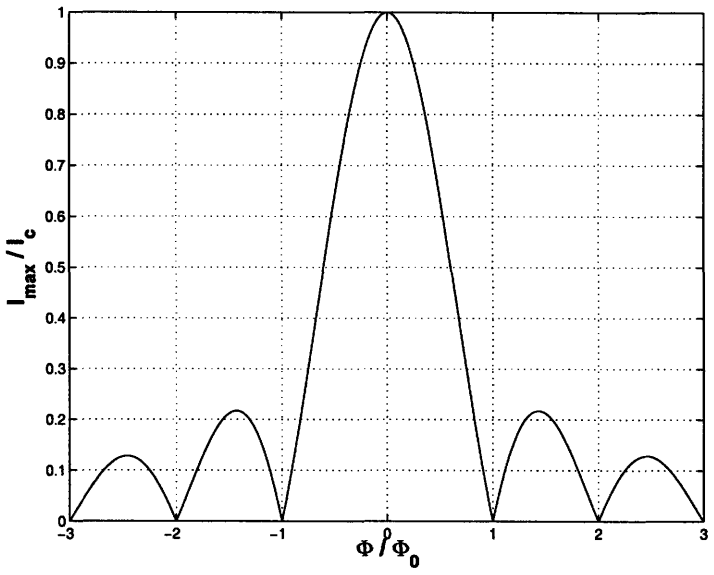

(a) Magnetic field on a Josephson junction

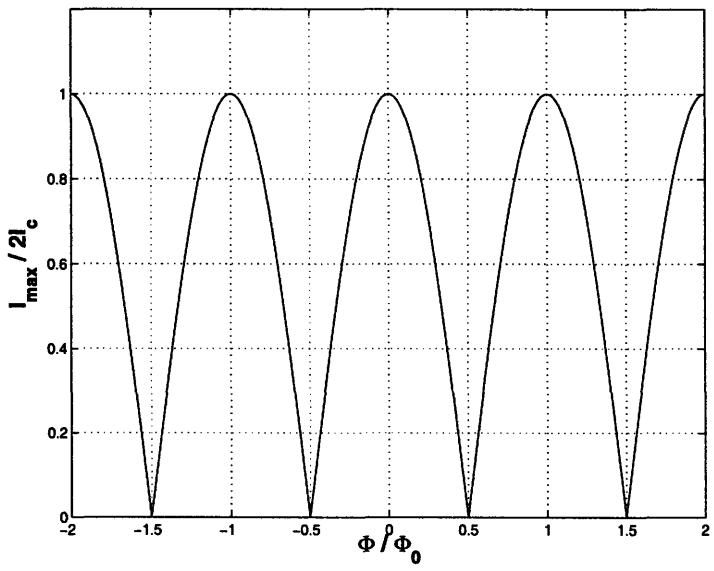

(b) Magnetic field on a SQUID

Figure 2-4: Magnetic field effects on the supercurrent. (a) The effect of a magnetic field on a Josephson junction's maximum supercurrent, where Φ is the flux across the junction; nodes occur at characteristic fields B_0, $2B_0$, $3B_0$, etc. (b) The periodic effect of a magnetic field on the maximum supercurrent for a SQUID; here, Φ refers to the flux through the entire superconducting loop. A SQUID is thus an excellent magnetometer for measuring integer multiples of the magnetic flux quantum, Φ_0.

Chapter 3

Characterizing Josephson Junctions

3.1 The Multi-Chip Probe

A major initiative at MIT Lincoln Laboratory has been concerned with testing Josephson junctions at room temperature (RT) and cryogenic temperatures (~4 K). The fabrication of these devices on wafers of chips continues to be improved through constant testing and analysis feedback. I initially started with analyzing data collected from a Peterson Probe, capable of testing a chip containing numerous Josephson junctions at RT or at 4 K. Much of this work was already accomplished and documented extensively by Keith Brown [29]. He developed MATLAB programs to characterize the current-voltage ($I-V$) readouts of tested junctions and deduce certain important parameters, such as the gap voltage, knee voltage, normal resistance, critical current, etc. His software was also able to screen valid junctions from those with more erratic behavior, such as leaky, shunted, resistive, shorted, and open junctions. I helped to build from Keith's existing software by slightly improving its code and embellishing on the analysis.

In characterizing Josephson junctions, however, my efforts have primarily concentrated on testing with a Multi-Chip Probe (MCP). The MCP can house up to two printed circuit boards (PCB), each of which contains seven individual chips. Each

chip contains 24 contact pads and 24 grounding pads, where each junction can be individually tested with a standard four-point test. A switching matrix connected to the device electronics allows one to control the four-point channels ($V+$, $I+$, $I-$, $V-$) for testing the junction of interest. After cooling the apparatus to 4 K in a ^{4}He dewar, an $I-V$ trace for each junction was recorded on an oscilloscope and saved by a computer. Data collected from the MCP was managed by Terry Weir as part of the Low Temperature Superconducting Electronics (LTSE) and Deep Submicron (DSM) programs at MIT Lincoln Laboratory. I designed my own MATLAB software that processed the MCP data, and likewise identified junctions as valid, leaky, shunted, resistive, shorted, or open. My programs also evaluated relevant junction parameters, which were all stored in a new database management system as well as used for subsequent aggregate analysis of entire wafers.

3.2 Current-Voltage Characteristics

I characterized the $I-V$ traces from MCP data in a similar manner to that already outlined by Keith Brown in his analysis of Peterson Probe data [29]. The MATLAB program I designed first screens for any null data and then for junctions that are open, short, or completely resistive. It then proceeds to categorize any shunted or leaky junctions before finally analyzing valid junctions. The program is based on searching for significant changes in slope in the $I-V$ trace; it attempts to detect the sub-gap voltage, V_{sg}, at the first inflection point as well as the knee voltage, V_{knee}, at the second inflection point. The energy gap parameter in terms of voltage can be deduced by the relation

$$\Delta = \frac{V_{sg} + V_{knee}}{4} = \frac{V_g}{2}. \tag{3.1}$$

Finally, the program models the linear Ohmic behavior at either ends of the $I-V$ trace to determine the normal resistance R_n. A sample $I-V$ trace analyzed with relevant parameters displayed for a valid junction is illustrated in Fig. 3-1(a).

All data for each test structure relating to junction diameter, critical current, normal resistance, sub-gap and knee voltages, etc., was collected in a novel MCP

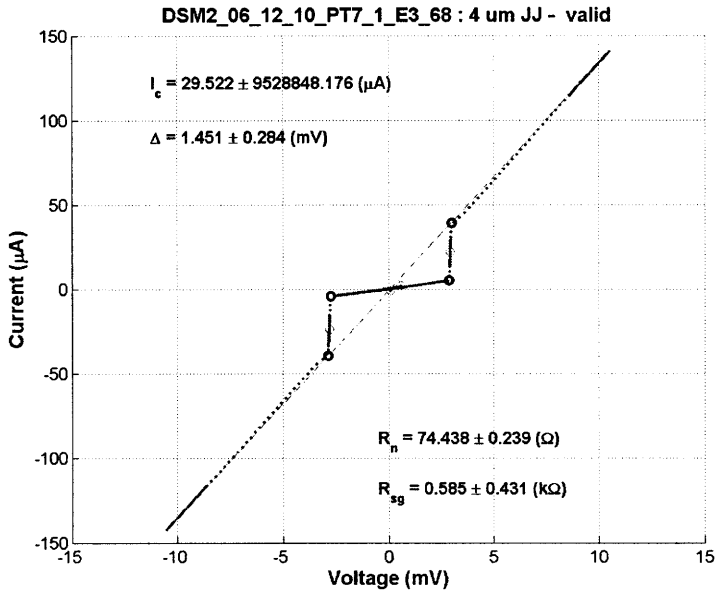

(a) $I - V$ trace

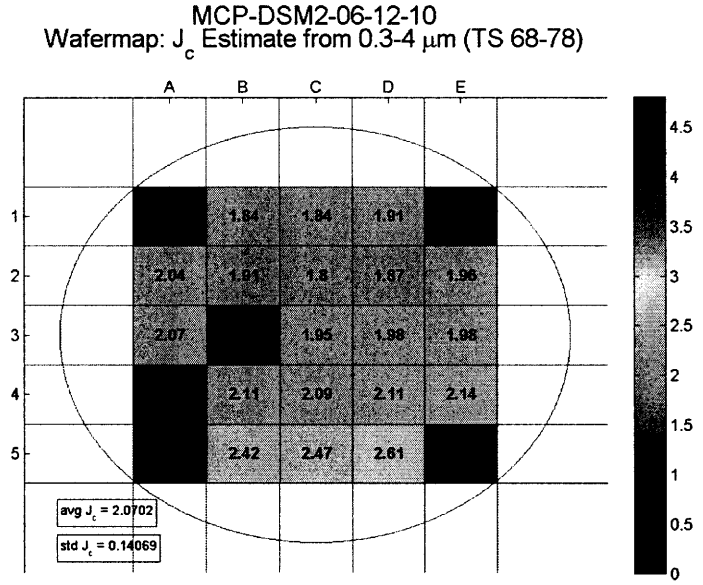

(b) J_c wafer map

Figure 3-1: MCP Analysis. (a) Sample $I-V$ trace of a valid 4 μm junction tested with the MCP, where inflection points V_{sg} and V_{knee} are indicated on the plot. Relevant parameters I_c, R_{sg}, and R_n are displayed. (b) Wafer map of J_c for various dice across wafer 06-12-10; a die with "NaN" indicates no junctions were tested.

database. As data for an entire wafer was accumulated in the database, an overall analysis was produced. A whole wafer comprises a 5×5 square array of dice (identified by columns A - E, rows 1 - 5) One of the several methods for surveying the wafer was to consider the critical current density, J_c, for each die across the wafer. A wafer map of J_c for wafer 06-12-10 is shown in Fig. 3-1(b). The various wafer maps and data summaries were very helpful towards observing the results of optical and process bias as well as towards redesigning more enhanced future DSM chips.

Chapter 4

Theory of Thermal Activation

4.1 The Washboard Potential

The theoretical models of Josephson junctions outlined in Sec. 2.4 are realized at the ideal temperature $T = 0$. We shall now like to investigate how thermal fluctuations can affect the dynamics of superconducting Josephson junctions. The phase of a Josephson junction resting in its energy potential is analogous to a mechanical bead situated on a corrugated washboard. In the absence of noise, the washboard is flat and the bead remains in one of the wells. This corresponds to the phase of a junction remaining in a potential well locked in the superconducting $V = 0$ state. Noise can cause the washboard to tip at an angle, however, allowing existing potential and kinetic energy to cause the bead to roll down into the neighboring well, or depending upon how tilted the washboard is, to continue running freely down the entire potential. This action represents the phase of the junction switching to the normal conducting $V \neq 0$ state with a maximum observed critical current $I_c < I_{c0}$, where I_{c0} is the ideal critical current at $T = 0$. There is a small probability of retrapping the phase in the next well, sustaining it in a $V = 0$ steady state, but we assume this probability to be negligible compared to the likelihood of transitioning into the $V \neq 0$ free-running state for some given time interval. [30][31]

The thermal activation model assumes a Stewart-McCumber circuit model for a Josephson junction in parallel with resistance R and capacitance C under a bias

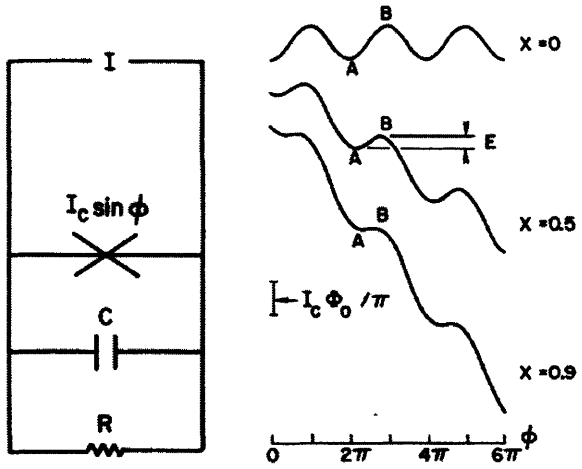

(a) The circuit model

(b) The washboard potential

Figure 4-1: Thermal activation theory was tested with these models. (a) The Stewart-McCumber circuit model contains a junction in parallel with a resistor R and capacitor C under the influence of a bias current I. (b) The washboard energy potential for the junction phase; the potential tilts at increasing angles for increasing values of $x = I/I_c$. The junction switches to the normal conducting state if it can thermally overcome the energy barrier E. (Figures reproduced from Fulton and Dunkleberger.)

current I (see Fig. 4-1(a)). We can use the Josephson equations

$$I = I_c \sin\phi + \frac{V}{R} + C\frac{dV}{dt}, \qquad 2\pi V = \Phi_0 \frac{d\phi}{dt} \tag{4.1}$$

to obtain the second-order differential equation

$$x = \frac{I}{I_c} = \sin\phi + \frac{1}{\omega_0^2 \gamma}\frac{d\phi}{dt} + \frac{1}{\omega_0^2}\frac{d^2\phi}{dt^2}, \tag{4.2}$$

where $\gamma = RC$ and $\omega_0 = (2\pi I_c/\Phi_0 C)^{1/2}$ is the natural frequency for the potential well. We represent the energy function as a cosine potential, where the potential is tilted at an angle proportional to the bias current I. If E denotes the energy barrier that must be overcome for the junction to switch from the initial superconducting $V = 0$ state to the normal $V \neq 0$ state, we can model the energy for some fixed I and I_c as

$$E = (I_c\Phi_0/2\pi)[x(2\sin^{-1}x - \pi) + 2\cos(\sin^{-1}x)]. \tag{4.3}$$

The theoretical model of E with respect to x is shown in Fig. 4-2. We notice that when no bias current is supplied ($x = 0$), the energy is at its maximum and corresponds to the steady superconducting state. However, as $x \rightarrow 1$, the energy E diminishes until there is no barrier sufficient to retain the ground superconducting state, and so the junction switches out to the normal conducting state.

4.2 Escape Rates

Sufficiently deep potential wells will confine the Josephson phase to the superconducting state. With the application of a bias current, however, we find the plasma frequency of oscillations in a potential well is given by

$$\omega_p = \omega_0(1 - x^2)^{1/4}. \tag{4.4}$$

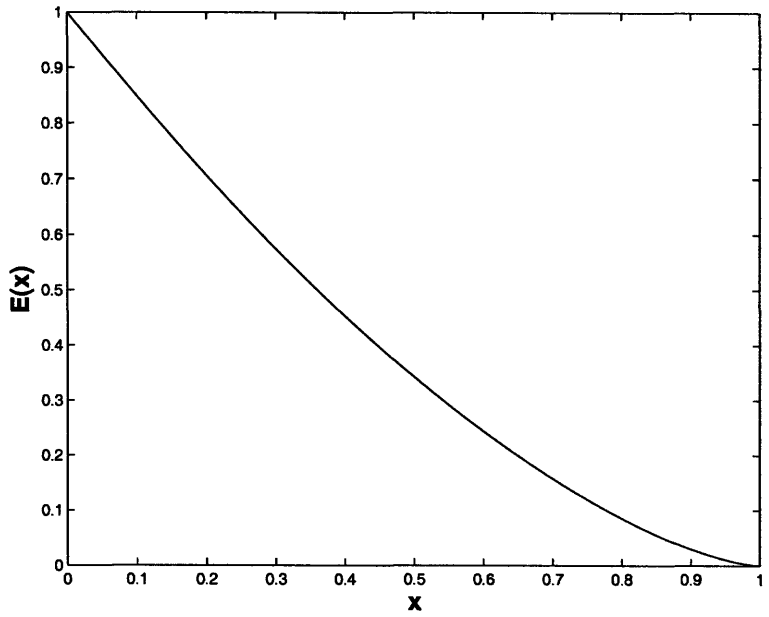

Figure 4-2: Theoretical dependence of E on $x = I/I_c$ (as given by Eq. 4.3) where E is expressed in units of $I_c\Phi_0/\pi$. (Figure adapted from Fulton and Dunkleberger.)

The damping factor is denoted by

$$Q = \omega_p RC. \tag{4.5}$$

In the regime $k_BT \gg \hbar\omega_p$, thermal activation can cause escape from a potential well to the free-running state where $d\phi/dt \propto V > 0$. Thus, the presence of thermal noise forces the junction to switch with an observed critical current I_c less than the ideal critical current I_{c0} of zero temperature. The escape rate for this thermal activation is a fundamental property of the junction for some fixed bias current [32]:

$$\tau_t^{-1} = \Gamma_t = a_t(\omega_p/2\pi)\exp(-E/k_BT). \tag{4.6}$$

The prefactor

$$a_t = 4/[(1 + Qk_BT/1.8E)^{1/2} + 1]^2 \tag{4.7}$$

is essentially unity for the underdamped limit, $\omega_0\gamma \gg 1$, which is the condition at which we tested the theory (Kurkijarvi has worked out the solutions for escape rates

in the high damping limit [33]). Finally, we observe that Eq. 4.6 altogether depends on the independent parameters of the critical current I_c, the capacitance C, the resistance R, and the temperature T.

For suitably low temperatures, quantum effects can dominate. The junction phase can quantum mechanically tunnel through the energy barrier and thus switch out to a $V \neq 0$ normal state. For the quantum realm ($k_B T \ll \hbar\omega_p$), wavefunction tunneling through the potential barrier occurs at a rate

$$\tau_q^{-1} = \Gamma_q = \frac{a_q \omega_p}{2\pi} \exp\left(-\frac{7.2E}{\hbar\omega_p}\left(1 + \frac{0.87}{Q}\right)\right) \tag{4.8}$$

where the prefactor $a_q \approx [120\pi(7.2E/\hbar\omega_p)]^{1/2}$ for the ideal $T = 0$. Notice that the temperature T does not appear in this equation since we expect to be in the ideal quantum state; thus, this model only relies on varying the three parameters I_c, C, and R.

Using the thermal activation and quantum mechanical tunneling models, Devoret *et al.* proposed expressing the escape rate in terms of an "escape temperature", T_{esc}, regardless of whether it was in the thermal regime or the quantum regime [32]. Thus, the two different escape rates can be commonly described by

$$\tau^{-1} = \Gamma = (\omega_p/2\pi)\exp(-E/k_B T_{esc}). \tag{4.9}$$

For the thermal regime, the escape temperature is

$$T_{esc} = \frac{T}{1 - p_t}, \tag{4.10}$$

where the factor $p_t = (k_B T/E)\ln a_t$ is negligible relative to unity, and in the quantum regime,

$$T_{esc} = \frac{\hbar\omega_p/k_B}{7.2(1 + 0.87/Q)(1 - p_q)}, \tag{4.11}$$

where $p_q \approx (\hbar\omega_p/7.2E)\ln a_q$.

4.3 The Switching Current Distribution

Supplying a specific bias current I causes a junction to switch at some observed current $I_{sw} < I_c$. However, stochastic processes due to randomness of noise-induced activation produce a broad distribution of possible values for I_{sw}. For a junction, each escape attempt of the phase out of the potential well is an independent event, mutually exclusive from any other attempt. Given that the plasma frequency is sufficiently high to afford very small escape interval times, the probability of escape for any attempt can be considered quite low. These criteria thus permit us to model the escape process using Poisson statistics [34]. A Poisson distribution characterizes the probability of statistically independent events at a time period t assuming the time interval Δt is adequately small. Thus, the probability of k random events in time interval t for a given rate Γ is characterized by

$$P(k,t) = \frac{(\Gamma t)^k e^{-\Gamma t}}{k!}. \tag{4.12}$$

In our study of switching current distributions, we ramp the bias current steadily from $I = 0$ up to some maximum current I_{max} and witness a switching event occur at some I_{sw}. We are interested in the current that is required to bring about the first switching event. In Poisson statistics, this probability is modeled exponentially as

$$f_{t_1}(l)\Delta t = \Gamma e^{-\Gamma t}\Delta t \tag{4.13}$$

where t_1 is the time until the first event. Now we can more constructively extend the Poisson mechanics to the switching current distribution of a junction under the influence of a ramped bias current. The average inter-arrival time, or average escape time, is simply the inverse of the escape rate: $\tau \equiv 1/\Gamma$. We want to consider the probability that the first switching event occurs at bias current I_{sw} within some current interval ΔI after ramping through a range of current values where no prior

switching event could have occurred. This probability is given as

$$f(I)\Delta I = P(I < I_{sw} \leq I + \Delta I) = P(A)P(B|A), \tag{4.14}$$

where A is the event that no switch has occured for any current up to I and B is the conditional event that the current then switches in the interval between I and $I+\Delta I$. Thus, we have

$$f(I)\Delta I = \frac{\Delta t}{\tau(I)}\left(1 - \int_0^I f(I')dI'\right), \tag{4.15}$$

or more elegantly

$$P(I) = \tau^{-1}(I)\left(\frac{dI}{dt}\right)^{-1}\left(1 - \int_0^I P(I')dI'\right), \tag{4.16}$$

where $\tau^{-1}(I)$ is the current-dependent escape rate, dI/dt is the ramp rate for the bias current, and $P(I)$ denotes the switching current probability distribution normalized to unity. To obtain the distribution experimentally, we ramp the current with a known sweep rate dI/dt and collect numerous samples to obtain a histogram of switching current values. Thus, knowing $P(I)$ and dI/dt, we can determine $\tau^{-1}(I)$ empirically, and using the theory of thermal activation discussed earlier, it will be possible to extract values for the critical current I_c, the capacitance C, the effective resistance R, and the temperature T.

Chapter 5

Modeling SQUID Dynamics

5.1 Experimental Methods

The SQUID device was fabricated at MIT Lincoln Laboratory and tested in collaboration with RLE. It was produced using a planarized Nb/Al/AlO_x/Nb trilayer process. The specific device was part of the DSM2 project, from run 05-19-08, die B4, chip 11, row 4, column 3. The device contains a SQUID with an inductively coupled qubit inside the SQUID loop. Although the device was primarily tested to monitor the qubit dynamics, I was investigating the performance of the SQUID. The SQUID possesses two equivalent-sized Josephson junctions fabricated with diameter 1.0 μm. Optical bias, however, indicated that the diameter was 1.11 μm, and process bias reduced the size by 0.43 μm. Thus, the effective diameter of the SQUID junctions at 4 K was $d = 0.68$ μm. The critical current density of the SQUID was measured at 4 K to be $J_c = 6.26$ μA/μm^2, with a normal resistance of $R_n = 395$ Ω. The qubit holds two Josephson junctions of equal size ($d = 0.79$ μm) with a third junction slightly smaller ($d = 0.74$ μm). An image of the SQUID/qubit assembly is shown in Fig. 5-1.

A circuit schematic of the device and testing apparatus is shown in Fig 5-2(a). The SQUID also contains a shunted 2 pF capacitor (SiO_x dielectric) to help detune noise-induced decoherence in the qubit. The device was tested with a ^{3}He dilution refrigerator. The sample was housed in an RF package with gold-plated copper

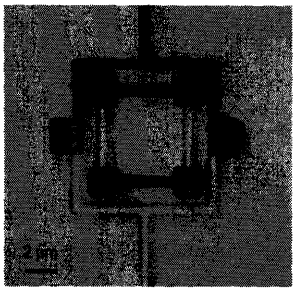

Figure 5-1: Optical micrograph of device. The SQUID is defined by the outer loop and the two parallel Josephson junctions. The inductively coupled qubit lies inside the SQUID loop with three Josephson junctions.

shielding. DC and RF input lines were soft-coaxial shielded cables connected with a bias-T. The DC lines were used to supply additional SQUID bias. Output lines also separated from a bias-T, and the readout was connected to a time interval analyzer. Copper powder filters were used for both input and output lines. A superconducting coil surrounds the RF package and was driven by a separate (magnet) current to penetrate the SQUID/qubit assembly with external flux (not shown in Fig. 5-2(a)). A thermometer was attached to the package to probe the device temperature. DC bias current sawtooth waveforms were produced by a signal generator at 100 Hz with 1 MΩ resistance. A computer controlled the readout from an oscilloscope and the spectrum analyzer.

5.2 Switching Current Distributions

For a particular magnetic frustration, a bias current was applied to the ground state of the SQUID through values marginally higher than the ideal critical current I_{c0} in order to ensure a switching event. The current was produced by a signal generator in the form of a triangle wavefunction (see Fig. 5-2(b)) at 1 MΩ resistance and 100 Hz frequency. Bias current for sample data collected at $T = 4.5$ K was produced with a voltage amplitude of 3.5 V, yielding a current ramp rate $dI/dt = 1.4$ mA/s. The time taken to switch from a zero voltage state to a non-zero voltage state, t_{sw}, was measured by a time interval analyzer and recorded by a computer. Ramping the

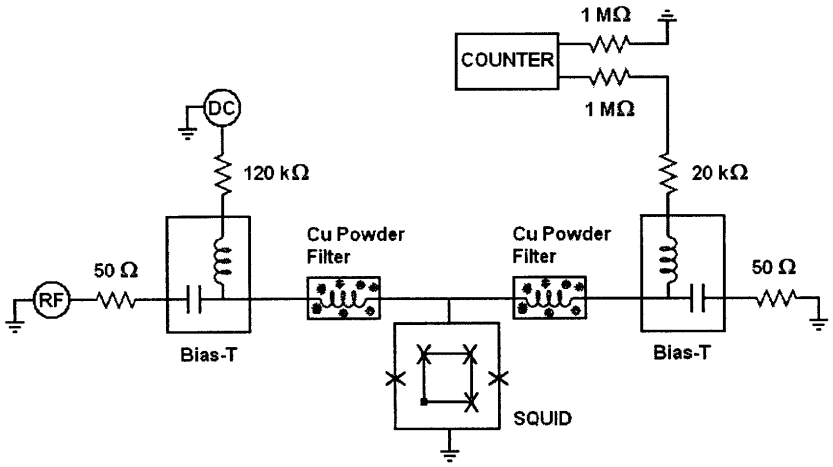

(a) Experimental setup

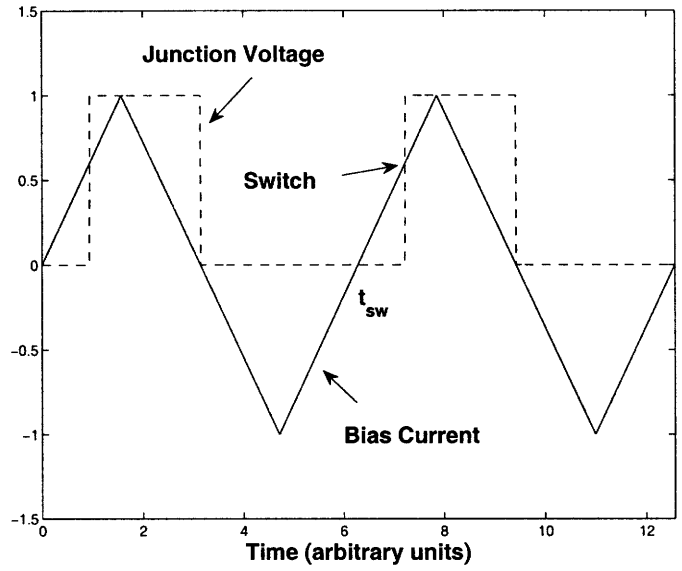

(b) Bias current waveform and junction voltage

Figure 5-2: Apparatus and data collection. (a) Circuit shematic of device and experimental setup. Copper powder filters are included before each bias-T, which serve to eliminate frequencies typically below 50 kHz. DC input lines provide SQUID bias. The readout is sent to a counter, or spectrum analyzer, from where data can then be sent to a computer for further analysis. An RF coil (not shown) driven by a magnet current surrounds the device package to supply magnetic flux. (b) Triangle waveform bias current with known ramping rate dI/dt. The junction switches from the zero voltage state at time t_{sw}, from which I_{sw} can be determined. The junction returns to the ground state when $I = 0$ and the process can be repeated.

current back down with the triangle waveform through $I = 0$ serves to retrap the SQUID to its resting zero-voltage ground state so the process can be repeated.

For a specific frustration applied, 10^5 samples were collected for statistical analysis. The switching times recorded were converted into switching current values I_{sw} knowing the ramp rate dI/dt. Finally, a histogram of I_{sw} was plotted using a suitable number of bins ($N = 150$) in order to afford a smooth probability curve $P(I)$. A

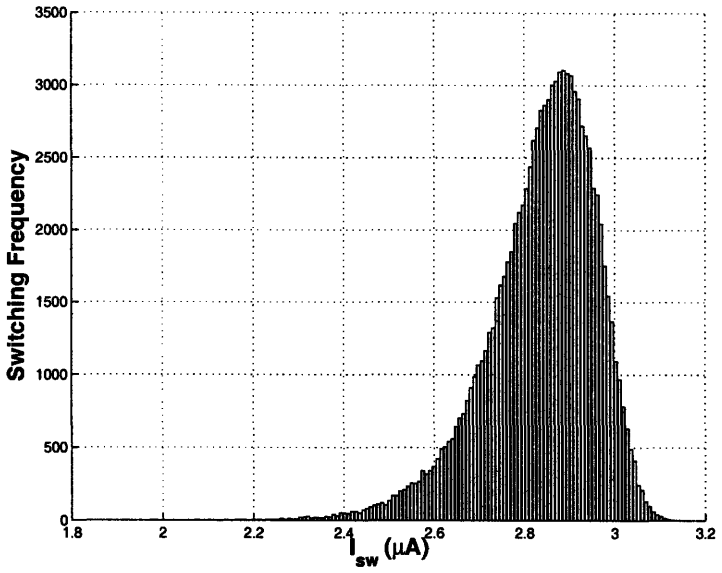

Figure 5-3: Thermal fluctuations result in a broad range of measured switching current values less than the critical current (4.88 μA); a smooth histogram (10^5 trials) of I_{sw} taken at $T = 4.5$ K is plotted with $N = 150$ bins.

sample switching current histogram for $T = 4.5$ K is shown in Fig. 5.2. We observe that the distribution is generally a bell-shaped curve that tapers off quite abruptly for $I/I_c \approx 1$. The critical current I_c for this trial (4.88 μA) would be slightly beyond the end of the histogram on the current axis. Thus, the sharp drop off represents that for such high currents near the critical current, an escape event has already likely occurred. The peak of the curve indicates the mean switching current.

With the experimentally acquired probability distribution $P(I)\Delta I$ (normalized to

unity), I numerically evaluated the escape rate $\tau^{-1}(I)$ using Eq. 4.16:

$$\tau^{-1}(I) = P(I)\left(\frac{dI}{dt}\right)\left(1 - \int_0^I P(I')dI'\right)^{-1}. \tag{5.1}$$

Plotting the escape rate τ^{-1} logarithmically with respect to I is easier for trying to correlate with theoretical models. Using thermal activation theory, I attempted to model the distribution according to Eq. 4.6 as

$$\ln(\tau^{-1}) = \ln(a_t) + \ln(\omega_p/2\pi) - (E/k_BT). \tag{5.2}$$

I programmed my fitting algorithm using custom-designed MATLAB software, for which the relevant code is provided in Appendix A. As previously mentioned, this fitting model relies on the freedom of four significant parameters: the critical current I_c, capacitance C, temperature T, and resistance R. Data points for the lowest and highest I/I_c values where the switching current histogram is relatively flat were excluded to only model the most uniform, non-deviating dataset (see Fig. 5-4(a)). We observe that $\ln(\tau^{-1})$ increases quite linearly with respect to I_{sw}; this relationship confirms the concept that escape rates (or escape probabilities) increase as the bias current is ramped up towards the critical current. The fitting algorithm attempts to iteratively solve for the relevant parameters I_c, C, T, and R from initial input estimates by optimizing mean-squared error reduction. Thus, the curve that optimally fits the points $\ln(\tau^{-1})$ plotted were used to determine the best parameters specified above. Finally, the acquired parameters were used to indirectly re-plot the distribution $P(I)\Delta I$ (using Eq. 4.16) against the measured switching current distribution to evaluate the effectiveness of this fitting method (see Fig. 5-4(b)).

5.3 Results and Discussion of Parameters

Data was collected with the same device at various temperatures ranging from 13 mK to 4.5 K. Initially for $T = 4.5$ K and 1.8 K, the fitting algorithm was found to be quite sensitive to the input resistance R. After testing through a wide range of

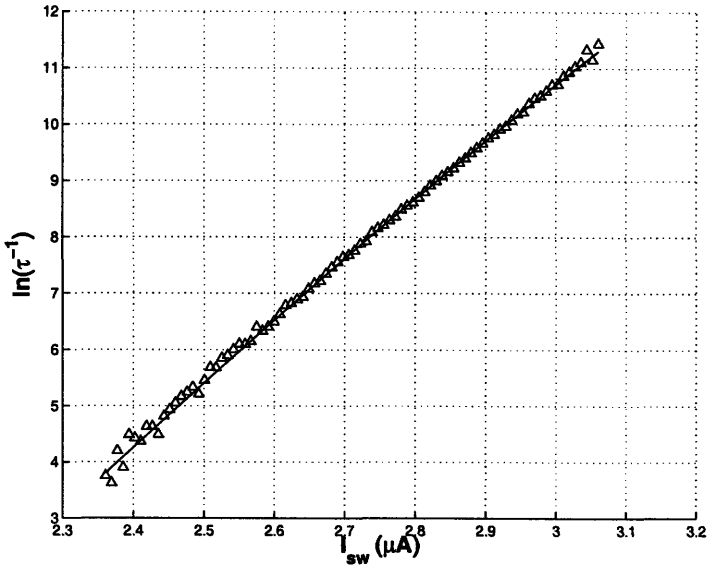

(a) Fitting model of $\ln(\tau^{-1})$

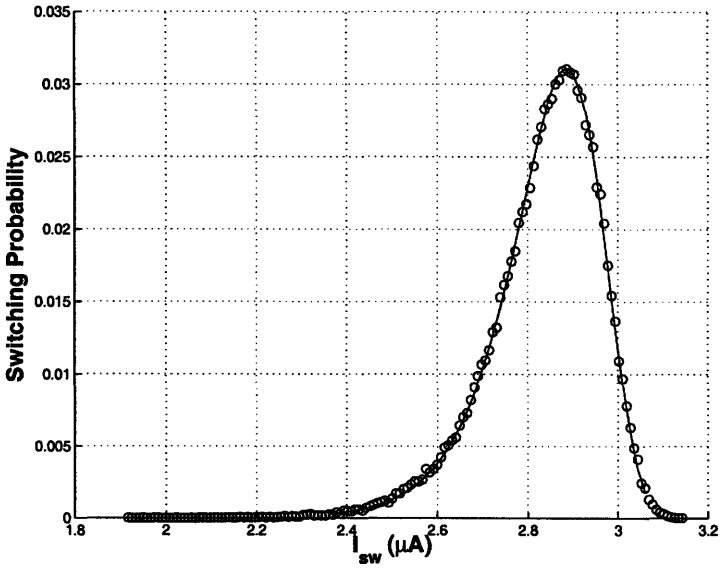

(b) Probability distribution model

Figure 5-4: Modeling the switching current. (a) Escape rates τ^{-1} plotted logarithmically against current for $T = 4.5$ K, with data points on either end excluded for fitting analysis. Relevant parameters were extracted from fitting with thermal activation theory. (b) Fit parameters from $\ln(\tau^{-1})$ vs. I_{sw} plot were used to retrace the model's switching current probability distribution over measured values.

values, a resistance of approximately 5 to 200 Ω was found to very accurately model the switching current distributions and still yield the other relevant parameters to within reasonable expectations. For $R > 200\ \Omega$, fitting parameters I_c and C deviated significantly from expected values. This range of R agrees with the effective parallel resistance experienced by the SQUID. From the schematic in Fig. 5-2(a), we note that the SQUID essentially experiences two 50 Ω resistors in parallel for an effective resistance of 25 Ω. Thus, the determined range for R is acceptable. Since the fitting algorithm essentially fixes the model to the value of R given as input, all subsequent analysis was simply fixed with input $R = 25\ \Omega$.

The thermal activation model fit the measured results with very good agreement. For the particular sample tested at 4.5 K shown in Fig. 5-4, the fitting model predicts, with small statistical error, the relevant parameters $I_c = 4.88\ \mu$A, $C = 2.00$ pF, and $T = 4.31$ K ($R = 24.98\ \Omega$). To summarize the 4.5 K test, 11 of the 19 equally spaced frustration points sufficiently high on the SQUID lobe were selected as valid samples for study. The results, given in Table 5.1, yielded acceptable values for the capacitance ($C = 1.990 \pm 0.004$ pF) and temperature ($T = 4.32 \pm 0.04$ K).

The device was also tested in a similar manner at 1.8 K, with the bias current ramped at $dI/dt = 3.2$ mA/s using a voltage amplitude of 8.0 V. Different levels of magnet current were applied, and 8 of 10 frustration points were deemed valid for analysis. Thermal activation theory succeeded in determining the capacitance $C = 2.000 \pm 0.002$ pF and the temperature $T = 1.86 \pm 0.06$ K very accurately (see summary of results in Table 5.1). It is interesting to demonstrate how the switching current distribution changes with respect to different applied frustration levels at the same temperature. A plot of switching current probability distributions for the eight different frustrations at 1.8 K, along with their fit models, is given in Fig. 5-5(a). The width of the distributions, relating to the error of the mean switching current value, stays relatively equal. The curve simply shifts along decreasing values of I_{sw} corresponding to decreasing I_c for the respective frustrations. The I_c values determined by the fitting model were plotted against the magnet current applied in Fig. 5-5(b), confirming the sinusoidal relationship given by Eq. 2.21.

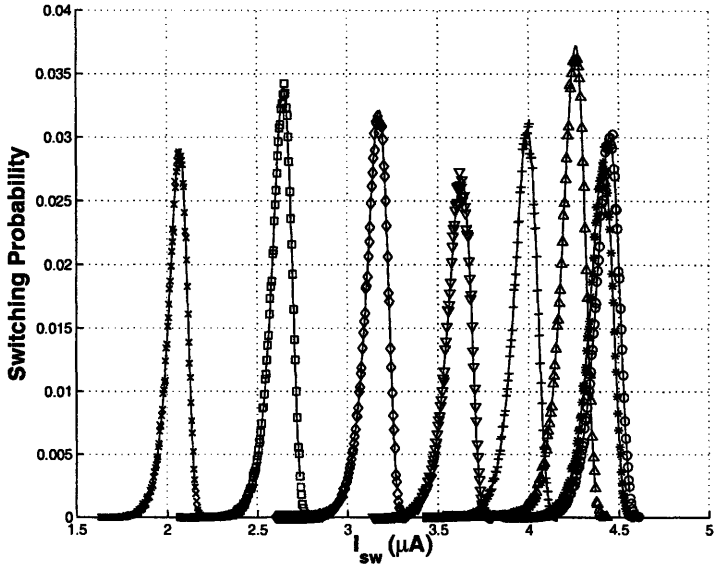

(a) Switching current distributions

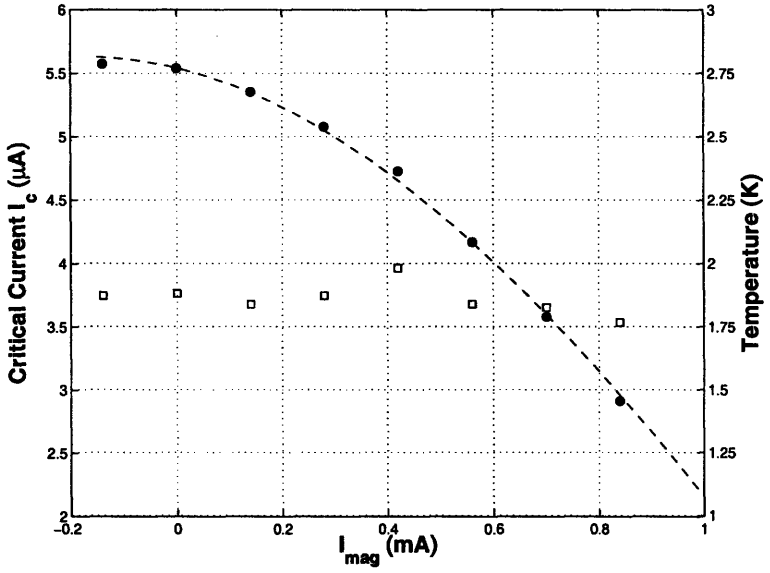

(b) Summary of I_c with frustration

Figure 5-5: $T = 1.8$ K. (a) Collection of switching current distributions for 8 different frustration points and their respective fit curves plotted. Frustrations increase from right to left. (b) Critical current I_c exhibits a general cosine relationship with the magnet current while the temperature T determined by the model stays the same.

Thermal activation theory has been well justified by the results at 4.5 K and 1.8 K. I was eager to model data at very cold temperatures in an attempt to investigate how well thermal activation theory could be used in the quantum regime. For $T =$ 13, 20, 31, and 57 mK, a voltage amplitude of 5.8 V was used to ramp a bias current at a rate $dI/dt = 2.32$ mA. Pure thermal activation models were able to adequately fit the data; the switching current distributions with their fit curves are shown in Fig. 5-6(a). Fixing $R = 25\ \Omega$ again for the model determined approximately the same $I_c = 5.312 \pm 0.009\ \mu$A and $C = 1.990 \pm 0.003$ pF. However, the temperatures obtained were significantly higher: 367, 371, 408, and 429 mK, respectively. It is likely that although the data could be fit sufficiently by the thermal activation model, the model does not accurately predict the correct parameters since we acquire an I_c less than the expected value ($\approx 5.5\ \mu$A) and much higher temperatures.

It is also possible that because we expect thermal activation theory to break down in the quantum regime, our attempts to model the cold temperature data are only met with temperatures much higher than their expected values. Ideally, the quantum model should be used to describe the escape rates; however, the quantum model makes no use of the temperature as it is expected to be at the ideal $T = 0$. Using expected values for $I_c = 5.5\ \mu$A, $C = 2.0$ pF, and $R = 25\ \Omega$, I illustrate the single defining quantum model alongside the switching current distribution for 13 mK in Fig. 5-6(b). The quantum model depicts a relatively sharp peak, and it would be difficult to fit the different cold temperature distributions with this one ideal quantum model.

This finding prompted us to test the device with a greater range of temperatures: 60, 100, 150, 200, 250, 300, 350, 400, 450, 500, 600, 700, 900, 1100, and 1800 mK. A bias current was produced from a voltage amplitude of 8.0 V, yielding a ramp rate $dI/dt = 3.2$ mA/s. For each temperature, typically 10 equally-spaced frustrations were applied to the device. I investigated the relationship between the temperature determined by the thermal activation fitting model, T_{fit}, and the expected experimental temperature T_{exp} across equivalent flux levels. This relationship is plotted in Fig. 5-7, along with the I_c determined by the fit model. The average critical current was found to be $I_c = 5.531 \pm 0.031\ \mu$A. The thermal activation model calculated

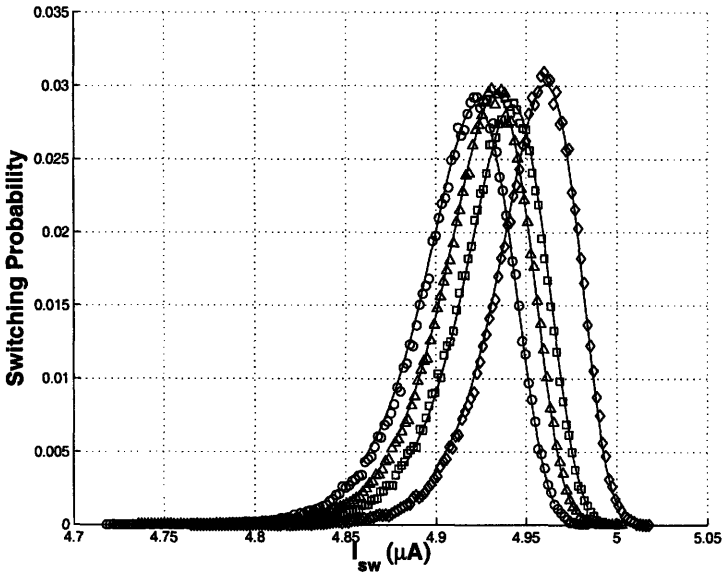

(a) Switching current distributions for low temperatures

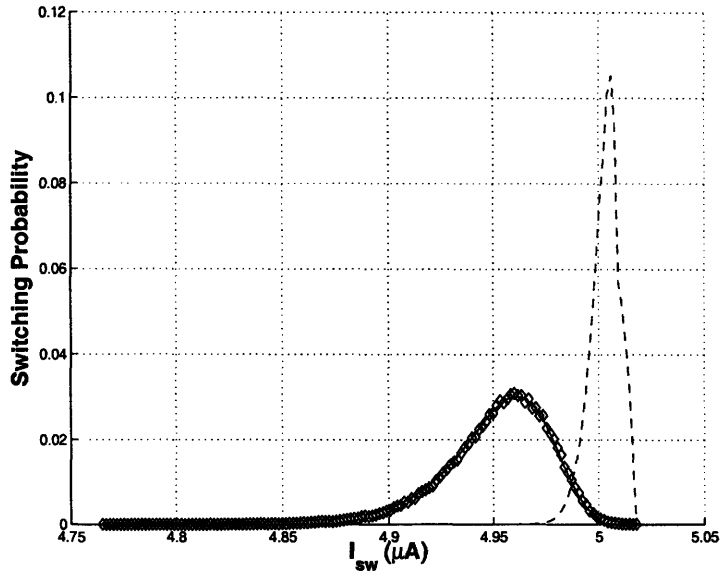

(b) Comparison with quantum model

Figure 5-6: Low temperature distributions modeled with thermal activation theory. (a) The thermal activation model was used to fit the switching current probability distributions at very low temperatures: 57 mK (○), 31 mK (△), 20 mK (□), and 13 mK (◇). (b) Thermal activation theory fit to 13 mK compared with the quantum mechanical tunneling model.

reasonable temperatures for most of the trials taken. For $T_{exp} \leq 300$ mK the model appeared to diverge more from the expected temperatures. For example, at the lowest temperature, $T_{exp} = 60$ mK while the model predicts $T_{fit} = 186$ mK, greater by a factor of three. It is reasonable to assume that a leveling effect is beginning to be observed at these low temperatures. This could mean that there is some intrinsic noise acting near base temperatures, or that the limits of the thermal model inhibit accurately describing the escape rates near the quantum regime. Attempts to model these low temperatures with a combined thermal and quantum model only allowed the thermal rates to dominate in the fitting scheme. A more prudent analysis that involves the quantum mechanical phenomena should be advanced in further investigations.

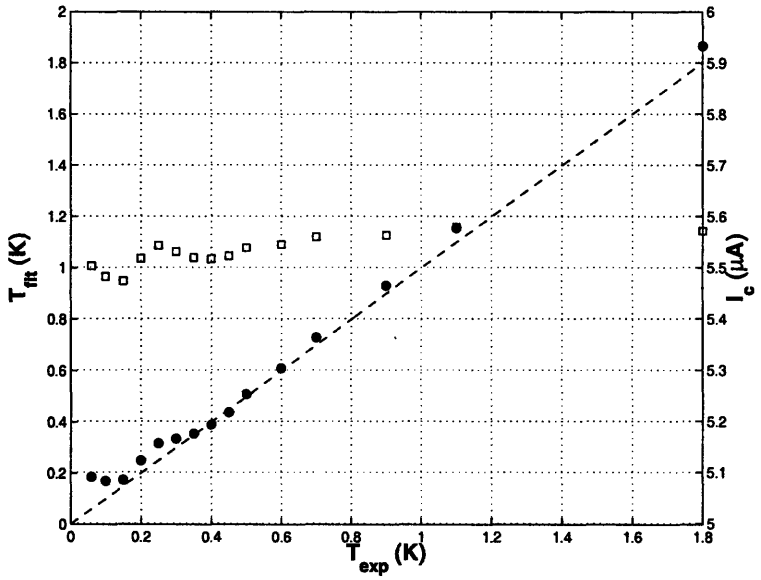

Figure 5-7: Temperatures determined by thermal activation theory, T_{fit}, were compared with expected, experimentally measured temperatures T_{exp}. The model seems to begin flattening out near 200-300 mK where noise fluctuations or the model limitations are met. The critical current, I_c, remained stable across temperatures for equivalent frustrations.

T_{exp}	I_c (μA)	C (pF)	T_{fit}
4.5 K	4.881	1.990 $\pm$ 0.004	4.32 $\pm$ 0.04 K
1.8	5.571	2.000 $\pm$ 0.002	1.86 $\pm$ 0.06
57 mK	5.318	1.993	428.7 mK
31	5.315	1.991	408.4
20	5.298	1.987	370.5
13	5.315	1.988	367.4
1100 mK	5.579	1.987	1154.8 mK
900	5.563	1.983	931.4
700	5.559	1.989	729.6
600	5.544	2.013	610.1
500	5.538	2.049	509.7
450	5.522	2.006	438.7
400	5.516	2.020	390.9
350	5.519	1.995	355.4
300	5.531	1.993	335.2
250	5.543	1.990	316.7
200	5.517	1.992	249.8
150	5.473	2.010	173.6
100	5.482	1.992	169.7
60	5.503	1.996	185.8

Table 5.1: Summary of Results. Fit parameters produced by thermal activation model/algorithm, where values for I_c are given only for zero frustration, and values for C and T_{fit} at T_{exp} = 4.5 K and 1.8 K are calculated across all frustration points tested.

Chapter 6

Future Work and Conclusions

6.1 Quantum Mechanical Tunneling

Modeling the SQUID dynamics under the influence of a bias current using thermal activation theory worked sufficiently well. The model was able to accurately predict the critical current, capacitance, resistance, and temperature within reasonable error. However, investigating the colder temperatures as we enter the quantum regime with $T \rightarrow 0$ reveals that thermal excitations alone are not sufficient to model the switching current probability and escape rates but that quantum mechanical tunneling must also be included. Although we can cool down our device electronics to base temperatures (~15 mK) with ^{3}He refrigeration, it would be impractical to assume that we can eliminate all sources of noise, thermal or otherwise. Therefore, modeling switching current distributions might require a combination of the thermal model and the quantum model where the escape rates owing to these processes would add to produce a total rate $\Gamma = \Gamma_t + \Gamma_q$. My attempts to combine these rates did not prove meaningful, since for a range of very low temperatures, the thermal activation model dominated in the fitting scheme. Also, because the quantum mechanical tunneling model is temperature-independent, for fixed I_c, C, and R, there is only a single distribution that results to describe the behavior. Future studies, however, require investigating exactly how switching current distributions should be modeled in the quantum regime to accurately describe the dynamics across a range of temperatures.

6.2 Summary and Conclusions

Noise excitations are of critical interest to the performance of Josephson junctions. Thermal activation results in a range of switching currents $I_{sw} < I_c$ for a SQUID tested under the influence of a bias current. After plotting a histogram of the switching currents, escape rates were plotted against current and were fit with the thermal activation model. Fit parameters of critical current I_c, capacitance C, resistance R, and temperature T were determined. The parameters were used to redraw the predicted switching current distributions over the measured results. At 4.5 K, a range of suitable resistance values was obtained that still permitted the model to fit the data well, so an input R was fixed at the expected 25 Ω. Different magnet currents applied at 1.8 K confirmed that the critical current I_c exhibits a cosine relationship with frustration while the temperature remains the same at $T = 1.86 \pm 0.06$ K. Finally, modeling thermal activation theory across different temperatures (at equivalent frustrations) shows the fitting model to work predominantly well, at least up to ~200 mK; the critical current was relatively unvarying at $I_c = 5.531 \pm 0.031$ μA. The quantum mechanical tunneling model should be better incorporated for a more accurate analysis of SQUID dynamics at extremely low temperatures (< 100 K).

Appendix A

MATLAB Code

The MATLAB program that I developed was used to test the thermal activation model, as well as the quantum tunneling model and combinations thereof, for switching current distribution data. The last function specified is a non-linear function fitting script borrowed and modified from the MIT Junior Physics Lab course (Scott Sewell), which follows the error analysis given in [35].

```
%%%%%%%%%%%%%%%%%%%%%%%%%%%%%%%%%%%%%%%%%%%%%%%%%%%%%%%%%%%%%%%%%%%%%%%%%%%%%%%
%%% Thermal Activation Model
%%% by Aditya Devalapalli (adevala@mit.edu)

function plotAverage2

%% opens gui dialog box to select the file; returns filename and full pathname
[fileName,pathName] = uigetfile('*.*','Select the dX_hist file for
                                                        average data');


numBins = 150;    %% set the number of bins (bars) in the histogram plot
ramprate = .0032; %% (A/s)
```

```
histFile = fullfile(pathName, fileName);
switch_time = load(histFile);

I = ramprate * switch_time;

[n,I_switch] = hist(I, numBins);
I_switch_raw = I_switch;
bar_fig = figure; hold on;
bar(I_switch*1e6,n); grid on;       %% produce bar histogram (unnormalized)
xlabel('I_{sw} (\muA)','FontSize',16,'FontWeight','bold');
ylabel('Switching Frequency','FontSize',16,'FontWeight','bold');
h = findobj(gca,'Type','patch');
set(h,'FaceColor','w','EdgeColor','k')

switch_fig = figure;
hold on;
norm_prob = n./sum(n);              %% normalized probability distribution
plot(I_switch*1e6,norm_prob,'bo');
grid on;
xlabel('I_{sw} (\muA)','FontSize',16,'FontWeight','bold');
ylabel('Switching Probability','FontSize',16,'FontWeight','bold');

binsize = I_switch(2) - I_switch(1);    %% binsize = Delta I in model

%%% calculate tau_inv and remove non-uniform points from further analysis
S = cumsum(norm_prob);

for i=1:length(S)
    if S(i) == 1
        S(i) = 0.99999;
```

```
    end
end

tau_inv_1 = norm_prob.*ramprate./(1-S)./binsize;

I_switch = I_switch(55:end-10);
tau_inv_1 = tau_inv_1(55:end-10);
S = S(55:end-10);

ind = find(tau_inv_1);
     % get rid of zeroes in tau_inv_1 so that log(tau_inv_1) doesn't mess up
tau_inv_1 = tau_inv_1(ind);
I_switch = I_switch(ind);
S = S(ind);

tau_inv_error = 1./sum(n).*ramprate./(1-S)./binsize;


%%%%%%%%%%%%%%%%%%%%%%%%%%%%%%%%%%%%%%%%%%%%%%%%%%%%%%%%%%%%%%%%%%%%%%%%%%%%%%%
%%% thermal activation
therm_fig = figure; hold on;
plot(I_switch*1e6,log(tau_inv_1),'r^');
grid on;

param = [5.5e-6 2e-12 1.8 25];    % estimate parameters
testSig = tau_inv_error./tau_inv_1;

[a_out,aerr,chisq,yfit] = fitnonlin(I_switch,log(tau_inv_1),testSig,
     'dunkleberger_thermal',param);
Final_Parameters = [a_out', aerr'];
```

```
I_c = a_out(1)
C = a_out(2)
T = a_out(3)
R = a_out(4)

% k_B = 1.3806505e-23;            % Boltzmann's constant
% phi_0 = 2.067833636e-15;        % flux quantum in Wb (SI units)
%
% x = I_switch./a_out(1);
% omega_J = sqrt(2*pi*a_out(1)/(phi_0*a_out(2)));
% omega_bar_J = omega_J*(1-x.^2).^(1/4);
% E = a_out(1)*phi_0/2/pi.*(x.*(2*asin(x)-pi)+2*cos(asin(x)));
%
% R = ((1-(2.*exp(-a_out(4)./2)-1).^2).*(1.8).*E)
          ./(omega_bar_J.*a_out(2).*k_B.*a_out(3));
% avg_R = mean(R)
% error_R = std(R)

RChiSquare = chisq/(length(I_switch)-length(a_out))

plot(I_switch*1e6,yfit,'b-');

xlabel('I_{sw} (\muA)','FontSize',16,'FontWeight','bold');
ylabel('ln(\tau^{-1})','FontSize',16,'FontWeight','bold');

% redraw distribution fit
P = exp(yfit)./ramprate.*(1-S).*binsize;
figure(switch_fig);
plot(I_switch*1e6,P,'r-');
```

```
%%%%%%%%%%%%%%%%%%%%%%%%%%%%%%%%%%%%%%%%%%%%%%%%%%%%%%%%%%%%%%%%%%%%%%%%%%%%
% %%% thermal activation / quantum tunneling
% switch_fig2 = figure;   hold on; %% normalized probability distribution
% plot(I_switch_raw*1e6,norm_prob,'bo');  grid on;
% xlabel('I_{sw} (\muA)','FontSize',16,'FontWeight','bold');
% ylabel('Switching Probability','FontSize',16,'FontWeight','bold');
%
% therm_fig2 = figure; hold on;
% plot(I_switch*1e6,log(tau_inv_1),'r^');
% grid on;
%
% param = [5.5e-6 2e-12 0.5];     % estimate parameters
% testSig = tau_inv_error./tau_inv_1;
%
% [a_out,aerr,chisq,yfit] = fitnonlin(I_switch,log(tau_inv_1),testSig,
                                  'devoret',param);
% Final_Parameters = [a_out', aerr'];
%
% I_c = a_out(1)
% I_c_error = aerr(1)
% C = a_out(2)
% C_error = aerr(2)
% T_esc = a_out(3)
% T_esc_error = aerr(3)
%
% RChiSquare = chisq/(length(I_switch)-length(a_out))
%
% plot(I_switch*1e6,yfit,'b-');
```

```
%
% xlabel('I_{sw} (\muA)','FontSize',16,'FontWeight','bold');
% ylabel('ln(\tau^{-1})','FontSize',16,'FontWeight','bold');
%
%
% %%% redraw distribution fit
% P = exp(yfit)./ramprate.*(1-S).*binsize;
% figure(switch_fig2);
% plot(I_switch*1e6,P,'r-');


%%%%%%%%%%%%%%%%%%%%%%%%%%%%%%%%%%%%%%%%%%%%%%%%%%%%%%%%%%%%%%%%%%%%%%%%%%%%%%%
% %%% quantum tunneling
% figure; hold on;
% plot(I_switch*1e6,log(tau_inv_1),'r^');
%
% a_input = [a_out(1) a_out(2) avg_R];
%
% test_theory = dunkleberger4(I_switch,a_input);
% plot(I_switch*1e6,test_theory,'b.-');
%
% testSig = tau_inv_error./tau_inv_1;
%
% [a_out,aerr,chisq,yfit] = fitnonlin(I_switch,log(tau_inv_1),testSig,
                                    'dunkleberger_quantum',a_input);
% Final_Parameters = [a_out', aerr'];
%
% I_c = a_out(1)
% C = a_out(2)
% R = a_out(3)
```

```
%
% figure(switch_fig);
% plot(I_switch*1e6,yfit,'g-');


%%%%%%%%%%%%%%%%%%%%%%%%%%%%%%%%%%%%%%%%%%%%%%%%%%%%%%%%%%%%%%%%%%%%%%%%%%%%%%%
function f = dunkleberger_quantum(I_switch,a)   %% pure quantum model

% a(1) = I_c
% a(2) = C
% a(3) = R

k_B = 1.3806505e-23;            % Boltzmann's constant
phi_0 = 2.067833636e-15;        % flux quantum in Wb (SI units)
hbar = 1.054571628e-34;         % Planck's constant in J*s

x = I_switch./a(1);
omega_J = sqrt(2*pi*a(1)/(phi_0*a(2)));
omega_bar_J = omega_J*(1-x.^2).^(1/4);
E = a(1)*phi_0/2/pi.*(x.*(2*asin(x)-pi)+2*cos(asin(x)));

Q = omega_bar_J.*a(3).*a(2);
a_q = (120.*pi.*(7.2).*E./hbar./omega_bar_J).^(1/2);

f = log(a_q) + log(omega_bar_J/(2*pi)) - (7.2).*E./hbar./omega_bar_J
                                                    .*(1+0.87./Q);

%%%%%%%%%%%%%%%%%%%%%%%%%%%%%%%%%%%%%%%%%%%%%%%%%%%%%%%%%%%%%%%%%%%%%%%%%%%%%%%
function f = dunkleberger_combined(I_switch,a)
                %% thermal and quantum rates added
```

```
% I_c = a(1);
% C = a(2);
% R = a(3);
% a_t = a(4);
% T = a(5);
% a_q = a(6);

k_B = 1.3806505e-23;            % Boltzmann's constant
phi_0 = 2.067833636e-15;        % flux quantum in Wb (SI units)
hbar = 1.054571628e-34;         % Planck's constant in J*s

x = I_switch./a(1);
omega_J = sqrt(2*pi*a(1)/(phi_0*a(2)));
omega_bar_J = omega_J*(1-x.^2).^(1/4);
E = a(1)*phi_0/2/pi.*(x.*(2*asin(x)-pi)+2*cos(asin(x)));
Q = omega_bar_J.*a(3).*a(2);

f = log(a(4).*(omega_bar_J/(2*pi)).*exp(-E./(k_B*a(5))) + a(6)
        .*omega_bar_J/(2*pi).*exp(-(7.2).*E./hbar./omega_bar_J.*(1+0.87./Q)));


%%%%%%%%%%%%%%%%%%%%%%%%%%%%%%%%%%%%%%%%%%%%%%%%%%%%%%%%%%%%%%%%%%%%%%%%%%%%
function f = dunkleberger_thermal(I_switch,a)   %% pure thermal model

% a(1) = I_c, the critical current
% a(2) = C, the capacitance
% a(3) = T, the temperature
% a(4) = log(a_t), a variable fit parameter --> determine R from this value
```

```
k_B = 1.3806505e-23;            % Boltzmann's constant
phi_0 = 2.067833636e-15;        % flux quantum in Wb (SI units)

x = I_switch./a(1);
omega_J = sqrt(2*pi*a(1)/(phi_0*a(2)));
omega_bar_J = omega_J*(1-x.^2).^(1/4);
E = a(1)*phi_0/2/pi.*(x.*(2*asin(x)-pi)+2*cos(asin(x)));

%%% include a(4) = R, the resistance
Q = omega_bar_J*a(4)*a(2);
a_t = 4./(((1+Q.*k_B.*a(3)./(1.8.*E)).^(1/2) + 1).^2);

f = log(a_t) + log(omega_bar_J/(2*pi)) - E./(k_B*a(3));

%%%%%%%%%%%%%%%%%%%%%%%%%%%%%%%%%%%%%%%%%%%%%%%%%%%%%%%%%%%%%%%%%%%%%%%%%%%%%%%
function f = devoret(I_switch,a)  %% basic model with escape temperature

% a(1) = I_c, the critical current
% a(2) = C, the capacitance
% a(3) = T_esc, the escape temperature

k_B = 1.3806505e-23;            % Boltzmann's constant
phi_0 = 2.067833636e-15;        % flux quantum in Wb (SI units)

x = I_switch./a(1);
omega_J = sqrt(2*pi*a(1)/(phi_0*a(2)));
omega_bar_J = omega_J*(1-x.^2).^(1/4);
E = a(1)*phi_0/2/pi.*(x.*(2*asin(x)-pi)+2*cos(asin(x)));

f = log(omega_bar_J/(2*pi)) - E./(k_B*a(3));
```

```
%%%%%%%%%%%%%%%%%%%%%%%%%%%%%%%%%%%%%%%%%%%%%%%%%%%%%%%%%%%%%%%%%%%%%%%%%%%%
function [a,aerr,chisq,yfit] = fitnonlin(x,y,sig,fitfun, a0)

% FITNONLIN Fit a nonlinear function to data using the gradient search
%           method discussed in Bevington and Robinson in Section 8.4.
%    [a,aerr,chisq,yfit] = fitnonlin(x,y,sig,fitfun,a0)
%
%    Inputs:  x -- the x data to fit
%             y -- the y data to fit
%             sig -- the uncertainties on the data points
%             fitfun -- the name of the function to fit to
%             a0 -- the initial guess at the parameters
%
%    Outputs: a -- the best fit parameters
%             aerr -- the errors on these parameters
%             chisq -- the final value of chi-squared
%             yfit -- the value of the fitted function
%                     at the points in x
%
%    Note: "fitfun" should be in a .m file similar to the
%    following example.
%
%          The following lines are saved in a file called
%          "sinfit.m", and the routine is invoked with
%          the fitfun parameter equal to 'sinfit' (including
%          the quotes)
%
%          function f = sinfit(x,a)
```

```
%          f = a(1)*sin(a(2)*x+a(3));
%

%****************************************
%*** Parameters you may need to modify ***
%****************************************
stepsize = abs(a0)*0.0001;
                % the amount parameters will be varied by in each iteration
chicut = 0.00001;
                % Maximum differential allowed between successive chi^2 values
silent = 1;
%****************************************
% These parameters can be varied if you have reason to believe your fit is
% converging to quickly or that you are in a local minima of the chi
% square.

stepdown = .1;
a = a0;

chi2 = calcchi2(x,y,sig,fitfun,a);
chi1 = chi2+chicut*2;

% keep looking while the value of chi^2 is changing
i=0;
while (abs(chi2-chi1))>chicut
    i=i+1;
    % Unless silent=1, the following is printed for each iteration:
    %   the current best fit parameters "a"
    %   the current chi-square "ChiSq"
    %   the change in the chi-square "diff"
```

```
  if silent~=1
    fprintf(1,'a = ');
    fprintf(1,'%f ',a);
    fprintf(1,'\t ChiSq = %f', chi2);
    fprintf(1,'\t diff = %f\n', abs(chi2-chi1));
    fprintf(1,'\n');
  end

  [anew,stepsum] = gradstep(x,y,sig,fitfun,a,stepsize,stepdown);
  a = anew;
  stepdown = stepsum;
  chi1 = chi2;
  chi2 = calcchi2(x,y,sig,fitfun,a);
end
i
%Unless silent=1, prints the last values after the minimum chi-sq has been
%found
if silent~=1
    fprintf(1,'a = ');
    fprintf(1,'%f ',a);
    fprintf(1,'\t ChiSq = %f', chi2);
    fprintf(1,'\t diff = %f\n', abs(chi2-chi1));
end


% calculate the returned values
aerr = sigparab(x,y,sig,fitfun,a,stepsize);
chisq = calcchi2(x,y,sig,fitfun,a);
yfit = feval(fitfun,x,a);
```

```
%-------------------
% the following function calculates the (negative) chi^2 gradient at
% the current point in parameter space, and moves in that direction
% until a minimum is found returns the new value of the parameters and
% the total length travelled

function [anew,stepsum] = gradstep(x,y,sig,fitfun,a,stepsize, stepdown)

chi2 = calcchi2(x,y,sig,fitfun,a);

grad = calcgrad(x,y,sig,fitfun,a,stepsize);

chi3 = chi2*1.1;
chi1 = chi3;

% cut down the step size in parameter space until a single step in
% the direction of the negative gradient yields a decrease in chi^2
stepdown = stepdown*2;
while chi3>chi2
  stepdown = stepdown/2;
  anew = a+stepdown*grad;
  chi3 = calcchi2(x,y,sig,fitfun,anew);
end
stepsum = 0;

% keep going in this direction until a minimum is passed
while chi3<chi2
  stepsum = stepsum+stepdown;
  chi1 = chi2;
  chi2 = chi3;
```

```
  anew = anew+stepdown*grad;
  chi3 = calcchi2(x,y,sig,fitfun,anew);
end
% approximate the minimum as a parabola (See Bevington p. 147).
step1 = stepdown*((chi3-chi2)/(chi1-2*chi2+chi3)+.5);
anew = anew - step1*grad;

%--------------------
% this function just calculates the value of chi^2
function chi2 = calcchi2(x,y,sig,fitfun,a)

chi2 = sum( ((y-feval(fitfun,x,a)) ./sig).^2);


%--------------------
% this function calculates the (negative) gradient at a point in
% parameter space (See Bevington p. 154).
function grad = calcgrad(x,y,sig,fitfun,a, stepsize)

f = 0.01;
[dum, nparm] = size(a);

grad = a;
chisq2 = calcchi2(x,y,sig,fitfun,a);

for i=1:nparm
  a2 = a;
  da = f*stepsize(i);
  a2(i) = a2(i)+da;
  chisq1 = calcchi2(x,y,sig,fitfun,a2);
```

```
  grad(i) = (chisq2-chisq1);
end

t = sum(grad.^2);
grad = stepsize.*grad/sqrt(t);

%-----------------
% this function calculates the errors on the final fitted
% parameters by approximating the minimum as parabolic
% in each parameter (See Bevington, p. 147).
function err=sigparab(x,y,sig,fitfun,a,stepsize)

[dum, nparm] = size(a);

err = a;
chisq2 = calcchi2(x,y,sig,fitfun,a);

for i=1:nparm

  a2 = a;
  da = stepsize(i);
  a2(i) = a2(i)+da;
  chisq3 = calcchi2(x,y,sig,fitfun,a2);
  a2(i) = a2(i)-2*da;
  chisq1 = calcchi2(x,y,sig,fitfun,a2);
  err(i)=da*sqrt(2/(chisq1-2*chisq2+chisq3));

end

%%%%%%%%%%%%%
```

Bibliography

[1] H. K. Onnes. *Leiden Comm.*, 120b, 122b, 124c, 1911.

[2] W. Meissner and R. Ochsenfeld. Ein neuer effekt bei eintritt der supraleitfahigkeit. *Naturwissenschaften*, 21(44):787–788, Nov 1933.

[3] J. Bardeen, L. N. Cooper, and J. R. Schrieffer. Theory of Superconductivity. *Phys. Rev.*, 108(5):1175–1204, Dec 1957.

[4] K. K. Berggren. Quantum computing with superconductors. *Proceedings of the IEEE*, 92(10):1630–1638, Oct 2004.

[5] T. P. Orlando, J. E. Mooij, Lin Tian, Caspar H. van der Wal, L. S. Levitov, Seth Lloyd, and J. J. Mazo. Superconducting persistent-current qubit. *Phys. Rev. B*, 60(22):15398–15413, Dec 1999.

[6] J. G. Bednorz and K. A. Muller. Possible high-T_c superconductivity in the Ba-La-Cu-O system. *Z. Phys. B*, 64(2):189–193, Jun 1986.

[7] M. K. Wu, J. R. Ashburn, C. J. Torng, P. H. Hor, R. L. Meng, L. Gao, Z. J. Huang, Y. Q. Wang, and C. W. Chu. Superconductivity at 93 K in a new mixed-phase Yb-Ba-Cu-O compound system at ambient pressure. *Phys. Rev. Lett.*, 58(9):908–910, Mar 1987.

[8] A. Schilling, M. Cantoni, J. D. Guo, and H. R. Ott. Superconductivity above 130 K in the Hg-Ba-Ca-Cu-O system. *Nature*, 363(6424):56–58, May 1993.

[9] D. Larbalestier, A. Gurevich, D. M. Feldmann, and A. Polyanskii. High-T_c superconducting materials for electric power applications. *Nature*, 414(6861):368–377, Nov 2001.

[10] J. Clarke. Principles and applications of SQUIDSs. *Proceedings of the IEEE*, 77(8):1208–1223, Aug 1989.

[11] J. Matisoo. Josephson-type superconductor tunnel junctions and applications. *IEEE Transactions on Magnetics*, 5(4):848–872, Dec 1969.

[12] Y. Yu, W. D. Oliver, D. Nakada, J. C. Lee, K. K. Berggren, and T. P. Orlando. Energy relaxation times in a Nb persistent current qubit. *IEEE Transactions on Applied Superconductivity*, 15(2):845–848, Jun 2005.

[13] Y. Yu, D. Nakada, J. C. Lee, B. Singh, D. S. Crankshaw, T. P. Orlando, K. K. Berggren, and W. D. Oliver. Energy relaxation time between macroscopic quantum levels in a superconducting persistent-current qubit. *Phys. Rev. Lett.*, 92(11):117904(4), Mar 2004.

[14] K. V. R. M. Murali, Z. Dutton, W. D. Oliver, D. S. Crankshaw, and T. P. Orlando. Probing decoherence with electromagnetically induced transparency in superconductive quantum circuits. *Phys. Rev. Lett.*, 93(8):087003(4), Aug 2004.

[15] D. S. Crankshaw and T. P. Orlando. Inductance effects in the persistent current qubit. *IEEE Transactions on Applied Superconductivity*, 11(1):1006–1009, Mar 2001.

[16] S. O. Valenzuela, W.D. Oliver, D.M. Berns, K.K. Berggren, L. S. Levitov, and T.P. Orlando. Microwave-induced cooling of a superconducting qubit. *Science*, 314(5805):1589–1592, Dec 2006.

[17] J.C. Lee, W.D. Oliver, T.P. Orlando, and K.K. Berggren. Resonant readout of a persistent current qubit. *IEEE Transactions on Applied Superconductivity*, 15(2):841–844, Jun 2005.

[18] W.D. Oliver, Y. Yu, J.C. Lee, K.K. Berggren, L.S. Levitov, and T.P. Orlando. Mach-Zehnder interferometry in a strongly driven superconducting qubit. *Science*, 310(5754):1653–1657, Dec 2005.

[19] D.M. Berns, W.D. Oliver, S.O. Valenzuela, A.V. Shytov, K.K. Berggren, L.S. Levitov, and T.P. Orlando. Coherent quasiclassical dynamics of a persistent-current qubit. *Phys. Rev. Lett.*, 97(15):150502(4), Oct 2006.

[20] T.P. Orlando, S. Lloyd, L.S. Levitov, K.K. Berggren, M.J. Feldman, M.F. Bocko, C. J. P. Mooij, J.E. Harmans, and C. H. Van der Wal. Flux-based superconducting qubits for quantum computation. *Physica C*, 372–376:194–200, Aug 2002.

[21] W. M. Kaminsky, S. Lloyd, and T. P. Orlando. Scalable superconducting architecture for adiabatic quantum computation, 2004.

[22] M. Tinkham. *Introduction to Superconductivity.* Krieger Publishing Co., 1975.

[23] L. Solymar. *Superconductive Tunneling and Applications.* Chapman and Hall, 1972.

[24] C. Kittel. *Introduction to Solid State Physics.* John Wiley & Sons, 8th edition, 2005.

[25] F. London and H. London. The electromagnetic equations of the supraconductor. *Proceedings of the Royal Society of London*, 149(866):71–88, Mar 1935.

[26] B. D. Josephson. Coupled superconductors. *Rev. Mod. Phys.*, 36(1):216–220, Jan 1964.

[27] V. Ambegaokar and A. Baratoff. Tunneling between superconductors. *Phys. Rev. Lett.*, 10(11):486–489, Jun 1963.

[28] S. Shapiro. Josephson currents in superconducting tunneling: The effect of microwaves and other observations. *Phys. Rev. Lett.*, 11(2):80–82, Jul 1963.

[29] K.A. Brown. *Cryogenic characterization of Josephson junctions.* Undergraduate physics thesis, Mass. Institute of Tech., 2006.

[30] T.A. Fulton and L.N. Dunkleberger. Lifetime of the zero-voltage state in Josephson tunnel junctions. *Phys. Rev. B*, 9(11):4760–4768, Jun 1974.

[31] R.F. Voss and R.A. Webb. Macroscopic quantum tunneling in 1-μm Nb Josephson junctions. *Phys. Rev. Lett.*, 47(4):265–268, Jul 1981.

[32] M.H. Devoret, J.M. Martinis, and J. Clarke. Measurements of macroscopic quantum tunneling out of the zero-voltage state of a current-biased Josephson junction. *Phys. Rev. Lett.*, 55(18):1908–1911, Oct 1985.

[33] J. Kurkijarvi. Intrinsic fluctuations in a superconducting ring closed with a Josephson junction. *Phys. Rev. B*, 6(3):832–835, Aug 1972.

[34] W.D. Oliver. Derivation of the critical current distribution function for Josephson junctions. Memorandum to MIT/Lincoln Laboratory, Apr 2003.

[35] P.R. Bevington and D.K. Robinson. *Data Reduction and Error Analysis for the Physical Sciences.* McGraw-Hill, 2nd edition, 1992.